SEISMIC RESPONSE OF TUNNEL STRUCTURE: EFFECT OF STRATIGRAPHY AND ASSESSMENT OF FRAGILITY CURVES

Submitted in partial fulfillment of the requirements for the award of degree of

Master of Technology

In

STRUCTURAL ENGINEERING

Submitted by

Komal Pareek

(2014PCS5126)

Supervised by

Dr. Rajib Sarkar

DEPARTMENT OF CIVIL ENGINEERING

MALAVIYA NATIONAL INSTITUTE OF TECHNOLOGY JAIPUR

JUNE 2016

A

DISSERTATION REPORT

ON

SEISMIC RESPONSE OF TUNNEL STRUCTURE: EFFECT OF STRATIGRAPHY AND ASSESSMENT OF FRAGILITY CURVES

Submitted in partial fulfillment of the requirements for the award of degree of

Master of Technology

In

STRUCTURAL ENGINEERING

Submitted by

Komal Pareek

Guided by

Dr. Rajib Sarkar
Assistant Professor

DEPARTMENT OF CIVIL ENGINEERING

MALAVIYA NATIONAL INSTITUTE OF TECHNOLOGY JAIPUR

JUNE 2016

©Malaviya National Institute of Technology Jaipur
All Rights Reserved

MALAVIYA NATIONAL INSTITUTE OF TECHNOLOGY JAIPUR

DEPARTMENT OF CIVIL ENGINEERING

JAIPUR 302017

DECLARATION

I hereby certify that the work which is being presented in the dissertation entitled "**SEISMIC RESPONSE OF TUNNEL STRUCTURE: EFFECT OF STRATIGRAPHY AND ASSESSMENT OF FRAGILITY CURVES**", in partial fulfillment of the requirements for the award of the Degree of Master of Technology and submitted in the Department of Civil Engineering of the Malaviya National Institute of Technology Jaipur is an authentic record of my own work carried out during a period from August 2015 to June 2016 under the supervision of Dr. Rajib Sarkar, Assistant Professor, Department of Civil Engineering, Malaviya National Institute of Technology Jaipur, India.

The matter presented in the thesis has not been submitted by me for the award of any degree of this or any other Institute.

(**KOMAL PAREEK**)

Student ID: **2014PCS 5126**

This is to certify that the above statement made by the candidate is correct to the best of my knowledge.

Dr. Rajib Sarkar
Assistant Professor
Dept. of Civil Engineering
MNIT Jaipur

ACKNOWLEDGEMENT

I owe a great thanks to a many people who helped and supported me during the project.

First and foremost, I would like to extend my deepest sense of gratitude and sincere appreciation to my senior Mr. Nishant Roy, PhD. Scholar, Department of Civil Engineering, MNIT Jaipur, for his constant guidance and encouragement without which this work would not have been possible.

I would also like to express gratitude and deep regards to my mentor Dr. Rajib Sarkar, Assistant Professor, Civil Engineering Department, MNIT Jaipur, for his exemplary guidance, monitoring and constant encouragement throughout the project. His supervision and willingness to share his vast knowledge has helped me to complete the assigned task.

I would also like to thank DPGC Convener, Prof. A. K. Vyas, Department of Civil Engineering, MNIT Jaipur, for extending every possible help and encouragement.

I would also like to offer my heartiest regards to Prof. Gunwant Sharma, Head of Department, Department of Civil Engineering, MNIT Jaipur.

I feel highly obliged to my parents for their everlasting support, which contributed towards the fulfillment of my studies. I also like to thank my younger brother Ankit Pareek for his love and concern for me.

My sincere thanks also go to all my friends who were encouraging me in accomplishing this work directly and indirectly. Special thanks to Swati Singh for her moral support and motivation which drives me to give my best.

(**KOMAL PAREEK**)

ABSTRACT

In mountainous terrain, tunnels play an important role in meeting increasing infrastructure demand of the region. Initially it has been assumed that tunnels, being surrounded by stable ground, are less vulnerable during seismic events but during recent earthquakes tunnels sustained severe damages. Therefore, the stability of tunnels during seismic events is a matter of great concern as any kind of failure may lead to interruption of traffic and adverse impact on regional economy.

Tunnels are generally constructed in stratified rock mass. Stratification leads to increase in vulnerability of tunnels in earthquakes due to transition zone between hard and soft rocks causing stiffness and seismic impedance mismatch. This causes differential kinetic movement and additional forces in tunnel liner leading to its failure. Therefore, in present study effect of stratigraphy is assessed by analyzing numerical model of tunnel located in single layer system and two layer geological set up.

As the seismic events are uncertain the assessment of the seismic risk in planning phase by examining vulnerability of tunnel through fragility curves or vulnerability curves is required. Fragility curves can be considered an emerging tool for analyzing performance of structures in earthquakes. Hence, this thesis aims to evaluate seismic fragility curves using numerical approach for tunnel support system which can be used for assessment of seismic risk and development of strategies for risk reduction.

LIST OF CONTENTS

LIST OF FIGURES

LIST OF TABLES

CHAPTER 1
INTRODUCTION

1.1 General

It is a general perception that underground structures such as tunnels are less vulnerable than over ground structures during seismic events as they are surrounded by ground. But during recent earthquakes such as 1999 Kocaeli (Turkey), 1999 Chi-Chi (Taiwan), 2004 Niigata (Japan) and 2008 Wenchuan (China), tunnels suffered severe damage. The common types of damages identified as buckling of steel reinforcements, lining cracks, lining spalling etc. Hence there is a need for assessment of performance of tunnels under earthquakes.

It has been identified that seismic vulnerability increases when tunnel passes through stratified rock mass due to amplified ground motion causing additional forces on tunnel support system. In order to investigate the influence of stratification, dynamic analysis has been performed on numerical model of tunnel using UDEC (Universal Distinct Element Code) and shear force, axial force and bending moments in tunnel liner has been compared for single layer and two layer geological set up.

The vulnerability of a structure can be assessed by fragility functions. Fragility functions relate ground motion parameter with probability of damage and constitute the main element of risk assessment. To assess the performance of tunnels fragility curves have been constructed for the tunnel liner considering the tunnel situated in stratified rock mass.

1.2 Objective of Thesis

Major goals of thesis are as follows-

1. Study of literature dealing with various methods of deriving seismic fragility curves for tunnel supports.
2. Understanding the basic modeling aspects and solution philosophy of distinct element method for static problems and carrying out validation study.
3. Understanding the modeling aspects for dynamic solution in discrete element method.

4. Investigate the effects of stratification on tunnel support system.
5. Construction of seismic fragility curves for tunnel support system.

1.3 Organization of the Thesis

Considering the objectives, the thesis is organized as follows.

Chapter 2 discusses various patterns of damage of mountain tunnels along with factors affecting damage. Methods for derivation of fragility curves have also been discussed.

Chapter 3 discusses the suitability of distinct element method for the present study. Formulation of distinct element method has been briefly discussed. Numerical method of derivation of fragility curve has been explained.

Chapter 4 describes the model adopted for the study. Seismic response of tunnel lining in single layer deposit and stratified (two-layer) deposit has been compared.

Chapter 5 represents seismic fragility curves for tunnel located in stratified deposit considering harmonic sinusoidal wave and earthquake time histories.

Chapter 6 provides a brief summary of thesis and recommendation need to be considered for the study.

CHAPTER 2
LITERATURE REVIEW

2.1 General

It has been assumed that tunnels experiences less damage from earthquakes in comparison to surface structures. However, studies conducted by Shen *et al.* (2014), Shimizu *et al.* (2007), Wang *et al.* (2001), Asakura *et al.* (2000) identified significant damage to mountain tunnels during earthquakes. This highlights the need of evaluation of performance of tunnels during seismic events. In present chapter various patterns of damage of mountain tunnels along with factors affecting damage have been described. A detailed description about fragility curves for tunnel supports has also been presented.

2.2 Damage to Mountain Tunnel

After Chi-Chi earthquake in central Taiwan Wang *et al.* (2001) carried out investigation for 57 tunnels and observed various types of damage to tunnels *e.g.*, portal failure, lining cracks, concrete lining spalling, cracks in pavement, collapse of lining due to failure of slope etc. Fig. 2.1 shows that most of the tunnels suffered damage due to cracks in concrete lining.

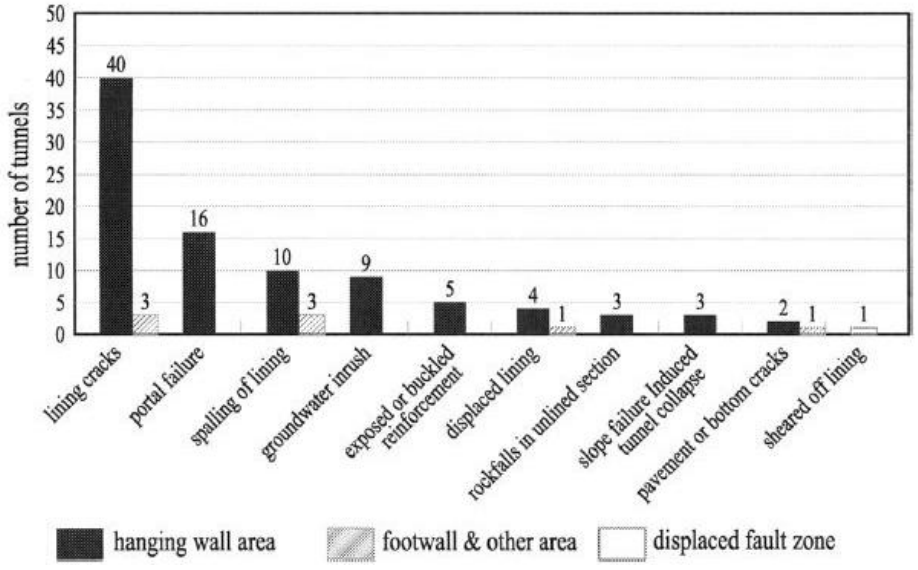

Fig. 2.1 Various types of tunnel damage during Chi-Chi earthquake (Wang *et al.*, 2001)

Shimizu *et al.* (2007) studied damage of mountain tunnels in Japan and based on the case studies classified damage patterns into three categories as represented in Fig. 2.2.

1. Damage of shallow depth tunnels- Tunnels constructed at shallow depth suffer more from earthquake as they are located in loose ground where seismic waves get amplified and deformation of ground is large.
2. Damage of tunnels of poor geological condition- When tunnels are located in fractured zone or soft ground, displacements due to seismic events are large causing severe damage to tunnels.
3. Damage of tunnels by slide of a fault – when earthquake fault crosses tunnels it causes compressive stresses, tensile stresses and shear stresses in tunnel lining and subsequently cracks in the lining.

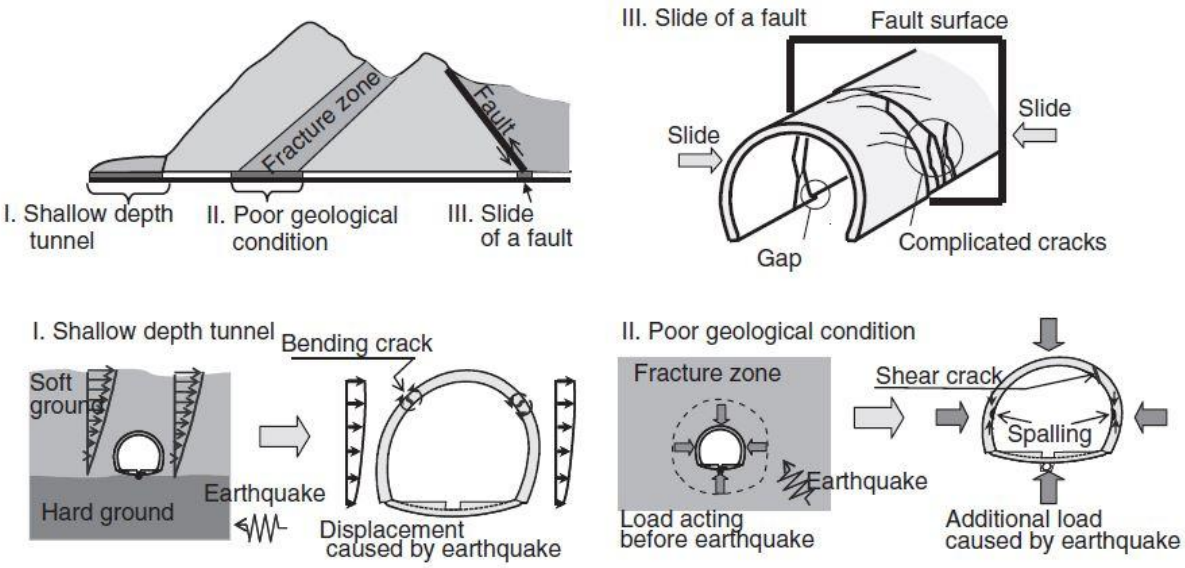

Fig. 2.2 Damage patterns of mountain tunnels **(**Shimizu *et al.* 2007)

Factors Affecting Tunnel Damage

There are various parameters on which damage of mountain tunnels depends. Some of the major factors identified by Wang *et al.* (2001) are-

1. Earthquake intensity at each tunnel – Earthquake intensity depends on the distance from the epicenter. It has also been observed that tunnel near the ground surface absorbs more energy due to reflection and refraction from ground surface.

2. Condition of the surrounding ground – As propagation of waves is faster in hard grounds so less energy of seismic waves is released in hard ground.

3. Seismic capacity of the tunnel - Tunnels having higher seismic capacity suffer less damage.

2.3 Methods of Deriving Fragility Curves

Fragility curves can be considered as a tool for assessment of performance of mountain tunnels. Fragility curves represent relation between ground motion parameter and damage. Various methods proposed for derivation of fragility curves are-

2.3.1 Analytical Method (Numerical Method)

Analytical fragility curves are derived by simulating idealized structural analysis models. The assumptions made during modeling and analysis is the main limitation of this method. The detailed procedure of construction of the analytical fragility curves is presented in section 3.4.

Mayoral *et al.* (2016) constructed fragility curves for tunnel shafts using numerical approach. The three-dimensional finite difference nonlinear analysis was performed using FLAC^{3D} program. The analysis was carried out for two types of soil profiles C & D as classified in Eurocode EC8. The seismic input with different frequencies was scaled up to 0.75 of PGA. The uncertainty in demand, capacity and damage state was considered. The results were extrapolated up to 1.5g considering nonlinearity to be increased with PGA. It was observed that the rate of damage decreases with seismic demand due to increase in damping.

Erberic (2008) derived fragility curves for masonry buildings classified into 120 classes based on structural parameters. Base shear capacity of masonry structures has been considered for damage state. From pushover and time-history analyses, capacity and demand curves have been constructed. Thereafter fragility curves have been derived indicating influence of material strength on probability of damage state.

2.3.2 Empirical Method

The empirical seismic fragility of structure represents the damage potential in future earthquakes. It can be assessed by statistical analysis of damage after occurrence of earthquake and the intensity of earthquake to which structure was subjected. The empirical fragility can be expressed either in terms of Damage probability matrixes (DPMs) or continuous fragility curves. The DPM represents the probability of particular level of damage when structure subjected to a particular level of intensity. And the probability of each column sums to 100%. The fragility curves are derived by fitting parametric statistical model according to observed data. The two forms of empirical fragility can be represented as shown in Fig. 2.3. Ioannow and Rossetto (2014) identified two factors on which reliability of empirical fragility functions depends: (a) quality of post-earthquake collected data and (b) the assumptions on which selected model is based upon.

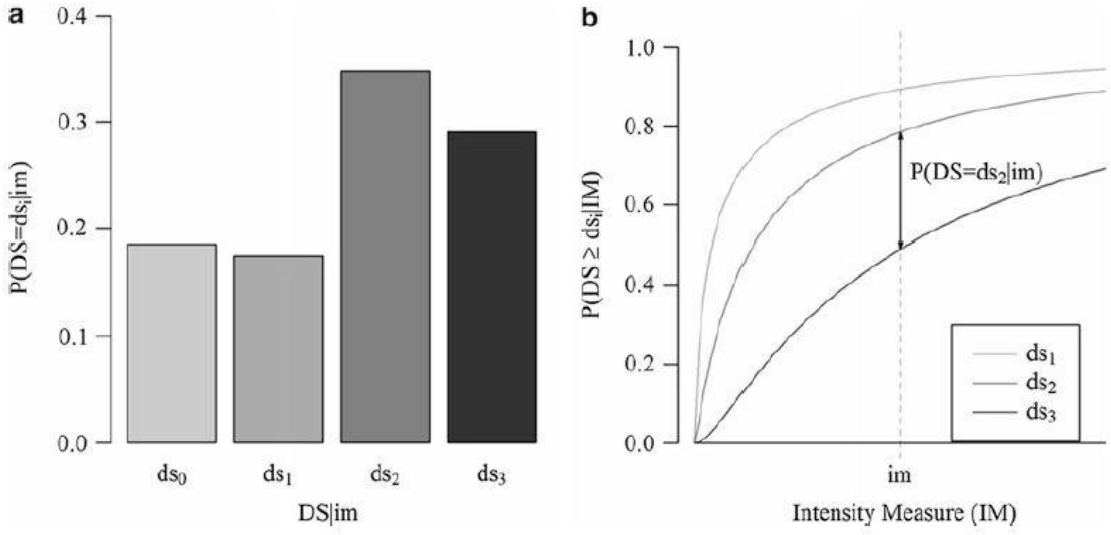

Fig. 2.3. Illustration of (a) a column of a DPM for intensity im, (b) fragility curves corresponding to n = 3 damage states for the same building class (Ioannow and Rossetto 2014)

The empirical method of fragility assessment was firstly introduced by Whitman *et al.* (1973). The data for the study was collected from 1240 questionnaires of the damage to buildings having 5 or more stories, caused by 9 February 1971, San Fernando earthquake, USA. They used empirical damage probability matrix (DPM) for their study. Eight damage scales ranging from 0

to 8 were used. Instead of a subjective description of physical damage, each damage state was identified by actual repair cost.

Rota *et al.* (2008) derived empirical fragility curves from data of Italian post-earthquake surveys of Abruzzo (1998), Irpinia (1980), Umbria-Marche (1997), Molise (2002) and Pollino (1998) earthquakes. The damage scale adopted for the study was similar to scale defined in European Macroseismic Scale. As the post-earthquake surveys were conducted at different time and for different earthquake so different damage scale converted into a unique one. The ground motion intensity was described by two parameters: PGA & Housner intensity (IH). Five damage levels were considered in addition to the case of no damage. First from the available empirical data damage probability matrixes were developed and then a lognormal probability distribution was fitted giving fragility curves.

Sarabandi *et al.* (2004) and King *et al.* (2004) derived empirical fragility curves for steel moment frame, wood frame, concrete frame, concrete shear wall and rehabilitated unreinforced masonry buildings. In order to see the effect of 1994 Northridge earthquake and 1999 Chi-Chi Taiwan earthquake, shaking on structures buildings located near strong ground motion recordings were inspected. The seismic performance level was characterized according to ATC-13, FEMA 273/356, HAZUS99, Vision 2000. From the observed data damage probability matrix and ground motion-damage relationship *i.e.* seismic fragility curves were derived.

2.3.3. Method Based on Expert Judgment

Based on the expert's estimates probability distribution function can be fitted relating damage and ground motion parameter of earthquake. As this method of derivation of fragility curve being completely depend on judgment of some expert is less reliable. This procedure is out-dated nowadays (SYNGER – G Reference Report, 2013).

CHAPTER 3
METHODOLOGY

3.1 General

Rapid advances in computer technology and sustained development have pushed numerical analysis approaches to the forefront of geotechnical practice. The various numerical approaches available for geotechnical investigations includes the FEM (Finite Element Method), FDM (Finite Difference Method), BEM (Boundary Element Method), DEM (Discrete Element Method), FDEM (Finite-Discrete Element Method) etc. In the present chapter, a brief discussion on the background of some of the widely utilised modelling approaches is presented. This is followed by a detailed description of the discrete element method (DEM) formulation which has been adopted in the present study. Applicability of the software used is validated by comparing results with analytical solutions. Moreover, a general discussion about evaluation of seismic fragility curves is presented for assessing the seismic vulnerability of the tunnel structure.

3.2 Different Methods for Numerical Modeling

3.2.1 Finite Element Method

FEM is very popular method of numerical modeling. The basic principle of this method is that the model is divided into finite number of elements which are connected together at nodes. Unknown parameters (*i.e.* displacements at nodes) are calculated and based on these, stresses are evaluated. It can handle anisotropy and nonlinearity of material, complex boundary conditions and any arbitrary shape of problem domain. Limitation of this method is that it is based on small strain theories and may not be adequate for large displacement problems. However, in case of jointed rock mass, large scale displacement in terms of sliding along the joints as well as block rotation and detachment is possible. Hence in such scenario, FEM has serious limitation.

3.2.2 Distinct Element Method

The Distinct Element Method was presented by Cundall (1971). In such formulation, the entire problem domain is treated as an assemblage of rigid or deformable blocks with discontinuities acting as interfaces. Large scale movement of blocks including rotation and detachment along the interface can be simulated making the approach versatile for adequately predicting the

response of jointed rock mass (Jing 2003). A more detailed description of a software package UDEC (Universal Distinct Element Method) utilized in the present study is presented below.

3.3 Universal Distinct Element Code (UDEC)

3.3.1 General

UDEC is a two dimensional numerical program for modeling of discontinuum media subjected to static or dynamic loading. Modeling in UDEC is based on Distinct Element Method (DEM). Calculation in UDEC is based on Lagrangian scheme and hence it is able to calculate large movements and deformations of a blocky system (Itasca *Inc*. 2004).

3.3.2 Formulation of UDEC

The solution process in UDEC is shown in Fig. 3.1 which is based on time stepping algorithm. To evaluate the response of the system force displacement law and Newton's second law of motion are used. Depending on the configuration of the system, the out of plane unbalanced force is evaluated for each block. The position of the blocks is then updated using laws of motion. Due to changed position new contacts are generated which are used to update the forces. While updating, the increment in normal and shear stress are considered as per Eq. 3.1 and Eq. 3.2.

$$\Delta\sigma_n = k_n \Delta u_n \tag{3.1}$$

$$\Delta\sigma_s = k_s \Delta u_s \tag{3.2}$$

where k_n = normal stiffness of interface; k_s = shear stiffness of interface.

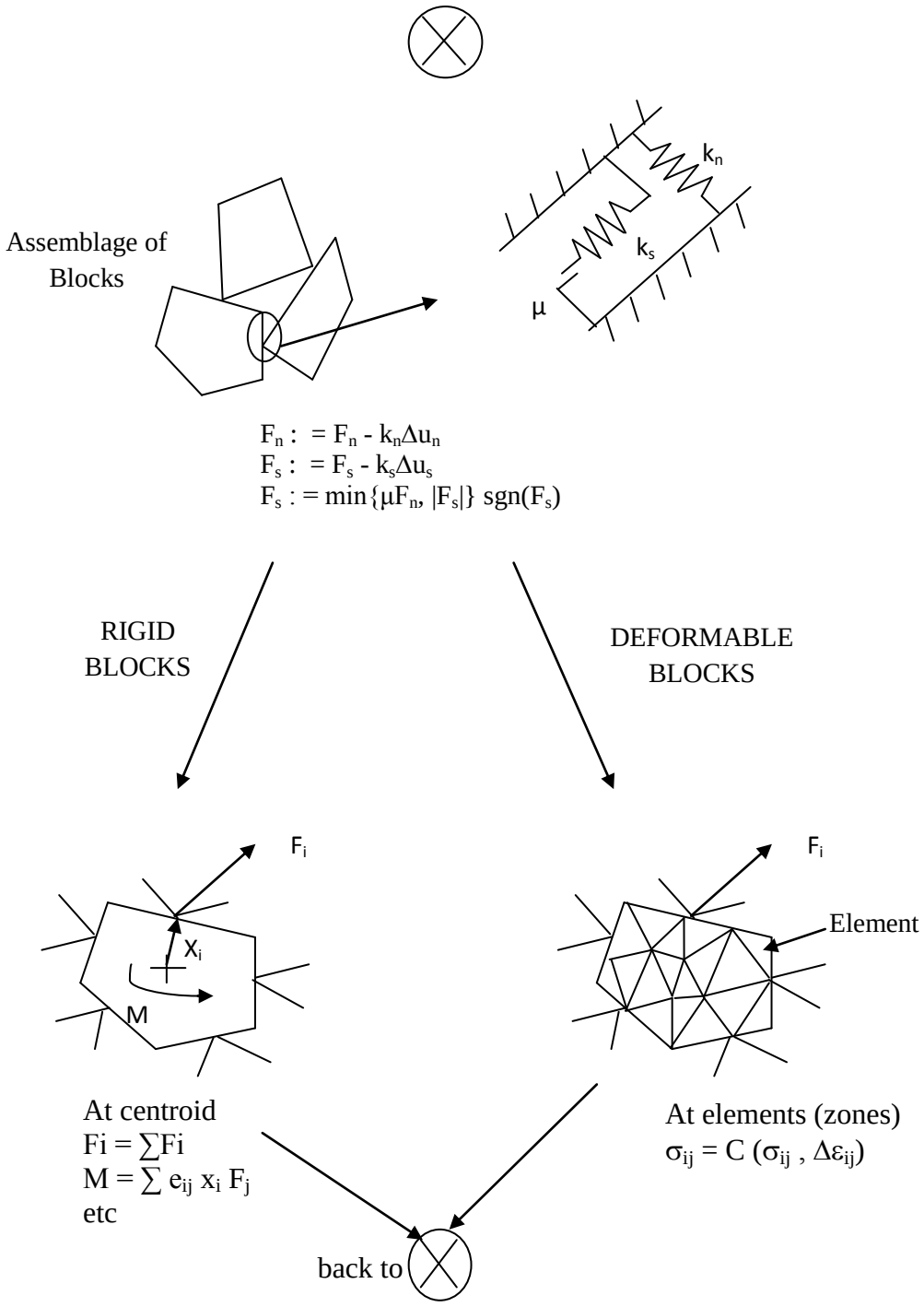

Fig. 3.1. Calculation cycle in distinct element method based formulation (Courtesy: Itasca *Inc*.)

3.3.3 Static Analysis using UDEC

The accuracy of the results predicted from any numerical analysis depends on a large number of factors. Some of the factors are related to model configurations which affect the accuracy including the mesh size, boundary conditions and model dimensions. The present section provides a brief description of the above factors.

Selecting appropriate zone size

The value of stresses and strains at any point evaluated in UDEC is the value at nearest grid point. In order to get accurate results, small mesh size should be used while generating zones. However, using very fine mesh result in additional computational burden and an increase in computation time. Hence based on the desired accuracy and sensitivity analysis, a suitable mesh size should be selected.

Boundary conditions

Boundaries of a numerical model can be classified as

a) *Real boundaries*: Real boundaries are stress free natural or excavated ground surface.
b) *Artificial boundaries*: These boundaries do not exist in reality but are provided to truncate the infinite extent of a real problem domain to include only area of interest in analysis and thus makes the simulation domain finite. These boundaries should be located such that it does not influence the results. Following two types of artificial boundaries are available in UDEC.

i) Prescribed displacement boundary - These boundaries are applied to inhibit movement of model either in horizontal or vertical direction or both.
ii) Prescribed stress boundary - In order to bring the model to equilibrium the horizontal stresses at the left and right boundaries are externally applied matching with initial stress state.

Validation of UDEC results for static analysis: Elastic plate (Kirsch solution)

In order to verify UDEC results, a homogenous rectangular elastic plate of dimensions 50 m x 50 m with a central hole of 2 m radius as shown in Fig. 3.2 is considered for analysis.

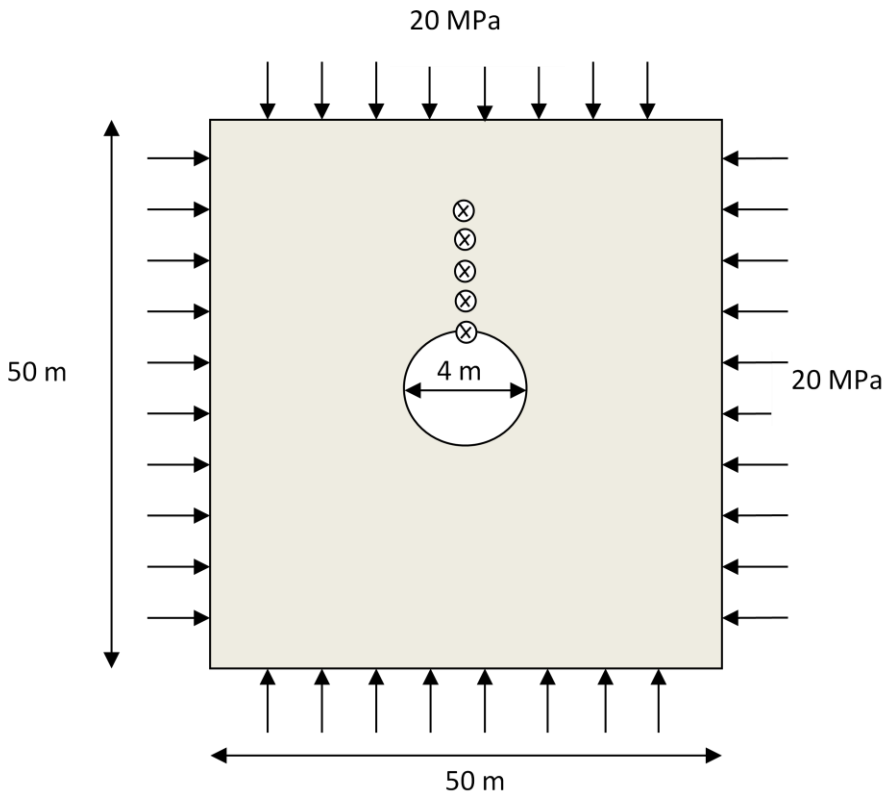

Fig. 3.2. Elastic plate used for validation study

The analytical solution for the distribution of stress in the radial and tangential direction derived by Kirsch (Goodman 1968) is shown in Eq. 3.3 and Eq. 3.4.

Radial Stress:

$$\sigma_r = \frac{P_1 + P_2}{2}\left(1 - \frac{a^2}{r^2}\right) + \frac{P_1 - P_2}{2}\left(1 - \frac{4a^2}{r^2} + \frac{3a^4}{r^4}\right)\cos 2\theta \tag{3.3}$$

Tangential stress:

$$\sigma_\theta = \frac{P_1 + P_2}{2}\left(1 + \frac{a^2}{r^2}\right) - \frac{P_1 - P_2}{2}\left(1 + \frac{3a^4}{r^4}\right)\cos 2\theta \tag{3.4}$$

In the numerical model, a compressive stress of 20 MPa is applied on all four boundaries. A mesh size of 0.3 m is adopted and model is run for sufficient number of cycles (i.e. 50,000) so that unbalanced system force becomes small and stable. The material properties adopted for the study are presented in Table 3.1.

Table 3.1. Material properties adopted for Kirsch solution

Density (kg/m^3)	Young's Modulus (GPa)	Poisson's Ratio
2000	12.4	0.24

The stresses in radial and tangential stresses are found at $\theta = 90^o$ and r = 2 m, 4 m, 6 m, 8 m and 10 m. Sufficiently finer mesh size has been used in the vicinity of the hole to get accurate results. Figs. 3.3-3.4 compare the numerical and analytical results showing a good agreement.

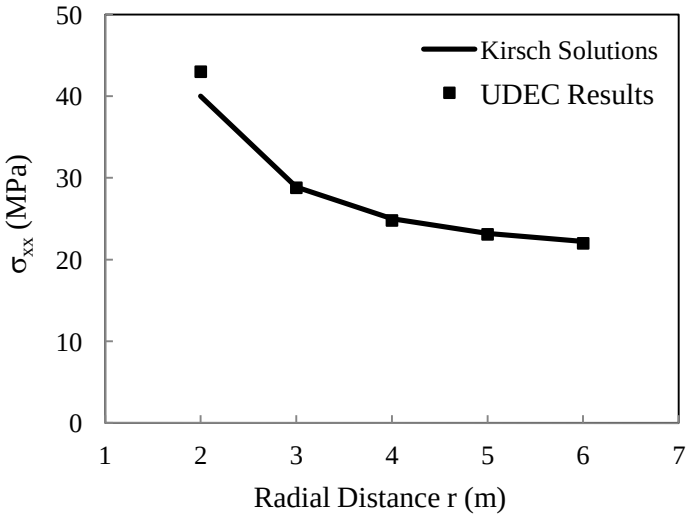

Fig. 3.3. Comparison of tangential stresses from UDEC with Kirsch solution

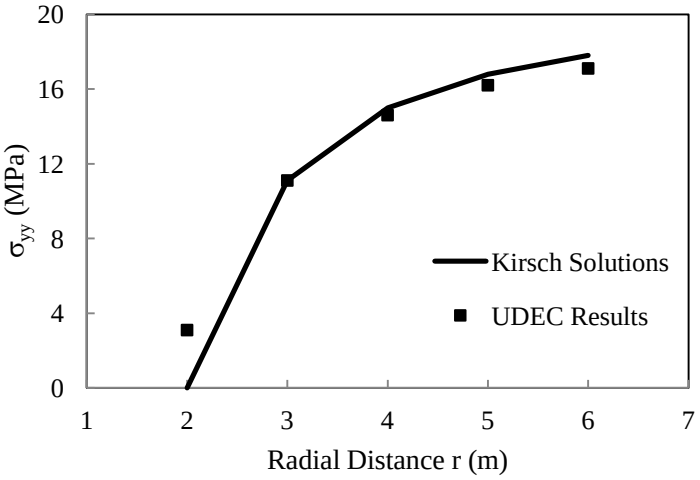

Fig. 3.4. Comparison of radial stresses from UDEC with Kirsch solution

3.3.4 Dynamic Analysis using UDEC

Dynamic numerical modeling of geotechnical problems poses a number of challenges because of the infinite extent of the problem domain and also the discretization of the problem domain. Artificial boundaries have to be incorporated in the numerical model along with special absorbing elements in order to simulate the infinite extent of the medium. Moreover, to ensure wave propagation through the geological medium without any distortion, the mesh size also has to be chosen judiciously. In the present section, some guidelines dealing with the above mentioned issues are highlighted.

Zone size

To ensure the propagation of dynamic waves without significant distortion, the mesh size should not be too large. Based on a number of studies carried out by researchers, mesh size smaller than 1/8 – 1/12 of the wavelength of the incident wave is suggested (Cai and Zhao 2000). Hence, in all the dynamic analysis, a mesh size falling in the above mentioned range was adopted to ensure minimal distortion of dynamic waves.

Boundary conditions

In dynamic analysis, artificial boundaries at the bottom and lateral sides of a numerical model should simulate transmitting nature replicating real scenarios. This requirement rules out the use of roller boundaries as they would cause wave reflection back into the model resulting in inaccurate results. At the same time, extending the boundaries to very large extent will make the analysis uneconomical by increasing the computational effort required. Hence, in order to minimize wave reflections from model boundaries either quiet boundaries (viscous boundaries developed by Lysmer and Kuhlemeyer 1969) or free field boundaries are used in UDEC.

Damping

As a part of energy loss, dynamic systems have some degree of damping. Two types of dynamic damping *i.e.* Rayleigh damping and local damping can be applied in UDEC.

Application of dynamic input

In UDEC a dynamic input can be applied in the model in following ways

a) *Velocity-history input (VHI)*: VHI cannot be applied along quiet (viscous) boundary condition. For applying VHI it is required to first fix the boundary along which dynamic wave is input. Fixed boundary is a reflective boundary so location of fixed boundaries should be decided judiciously as wave reflected from such boundaries may lead to scrupulous results.

b) *Stress-history input (SHI)*: An alternative method to input dynamic wave is with the SHI boundary condition. SHI does not require fixed boundaries but can be applied along quiet (viscous) boundary which absorbs incoming waves simulating the transmitting nature of infinite medium. In this method, the velocity records are converted into stress records by using Eq. 3.5 and Eq. 3.6 (Itasca *Inc.*, 2004).

$$\sigma_n = 2\rho C_p v_n \tag{3.5}$$

$$\sigma_s = 2\rho C_s v_s \tag{3.6}$$

Here a factor of two is applied because dashpots provide following viscous normal and shear stresses.

$$\sigma_n = -\rho C_p v_n \tag{3.7}$$

$$\sigma_s = -\rho C_s v_s \tag{3.8}$$

Where σ_n = applied normal stress; σ_n = applied shear stress; ρ = mass density;

C_p = speed of p-wave propagation through medium;

C_s = speed of s- wave propagation through medium;

v_n = input normal particle velocity;

v_s = input shear particle velocity

C_p and C_s are given by

$$C_p = \sqrt{\frac{K + 4G/3}{\rho}} \tag{3.9}$$

$$C_s = \sqrt{\frac{G}{\rho}} \tag{3.10}$$

Where K and G are bulk and shear modulus respectively.

3.4 Fragility Curves

Fragility curve is a tool for seismic risk assessment. It expresses probability of damage of structural/geotechnical system to reach or exceed certain damage state for a given ground motion intensity. Fragility curves are very significant for geotechnical structures as they form basis for risk analysis and risk reduction. The fragility curves allow to make assessment of damage to geotechnical systems from earthquake and helps in deciding retrofitting strategies. In this section, method of derivation of fragility curves is discussed in detail along with discussion of all the parameters required to develop fragility curves.

3.4.1 Elements of Fragility Curves

The procedure of derivation of fragility curves consists of: definition of system used, definition of ground motion parameter, evaluation of model and statistical processing of the results obtained from model analysis. The definition of damage state is also a key parameter for deriving fragility curves. The major elements of fragility curves are-

Intensity measure

The horizontal axis of fragility curve represents the level of ground motion associated to a certain value of probability of damage. Some of the proposed parameters are peak ground acceleration (PGA), peak ground velocity (PGV), spectral acceleration, spectral displacement, Housner intensity etc. After comparing these parameters Rota *et al.* (2008) suggests PGA as the most suitable one.

Performance level (Damage state)

The most common way to classify the performance level of structure is in terms of damage states: No damage, minor, moderate, extensive and complete damage. The damage state is user defined based on the experience and judgment of damage. In the present study six damage states are characterized which are presented in Table 3.2.

Table 3.2. Description of damage state considered for derivation of fragility curves

Damage state (ds_i)	Range of Damage Index	Central value of damage index
ds_0	DI ≤0.875	-
ds_1	0.875 < DI ≤ 1.125	1.00
ds_2	1.125 < DI ≤ 1.375	1.25
ds_3	1.375 < DI ≤ 1.625	1.50
ds_4	1.625 < DI ≤ 1.875	1.75
ds_5	DI > 1.875	-

3.4.2 Common Form of Fragility Function

Fragility function is commonly assumed to be the lognormal cumulative distribution function which means that natural logarithm of fragility function is normally distributed. Eq. 3.11 gives its probability density function which can be reduced to Eq. 3.12 representing most common form of fragility function.

$$f(x) = \frac{1}{S\beta\sqrt{2\pi}} \cdot e^{-\frac{(\ln(S/S_{mi}))^2}{2\beta^2}} \tag{3.11}$$

$$P_f(d_s \geq d_{S_i} \mid S) = \phi\left[\frac{1}{\beta_{tot}}.\ln\left(\frac{S}{S_{mi}}\right)\right] \tag{3.12}$$

where P_f is the probability of reaching or exceeding a particular damage state d_s for a given seismic intensity level S (*i.e.* PGA), ϕ is the standard cumulative probability function, S_{mi} is the median threshold value of earthquake intensity measure corresponding to the i^{th} damage state. β_{tot} is the total lognormal standard deviation.

3.4.3 Determination of Parameters

For development of fragility curves it is required to determine the values of two parameters namely total standard deviation β_{tot} and earthquake intensity measure corresponding to a particular damage state S_{mi}.

Determination of β_{tot}

β_{tot} is defined as the total variability associated with fragility curve which is combination of three terms: β_C denoting the variability of capacity of tunnel, β_D representing the variability of seismic demand and β_{DS} which signifies the uncertainty on the definition of damage state. Thus, β_{tot} is given by Eq. 3.13.

$$\beta_{tot} = \sqrt{\beta^2{}_{DS} + \beta^2{}_{C} + \beta^2{}_{D}} \tag{3.13}$$

The value of β_{DS} is taken as 0.4 and that of β_C is taken as 0.3 (Argyroudis and Pitilakis, 2012). β_D is the average standard deviation of plot of damage index on natural log scale (*i.e. ln DI*) versus PGA on natural log scale (*i.e. ln PGA*) as represented in Fig. 3.5.

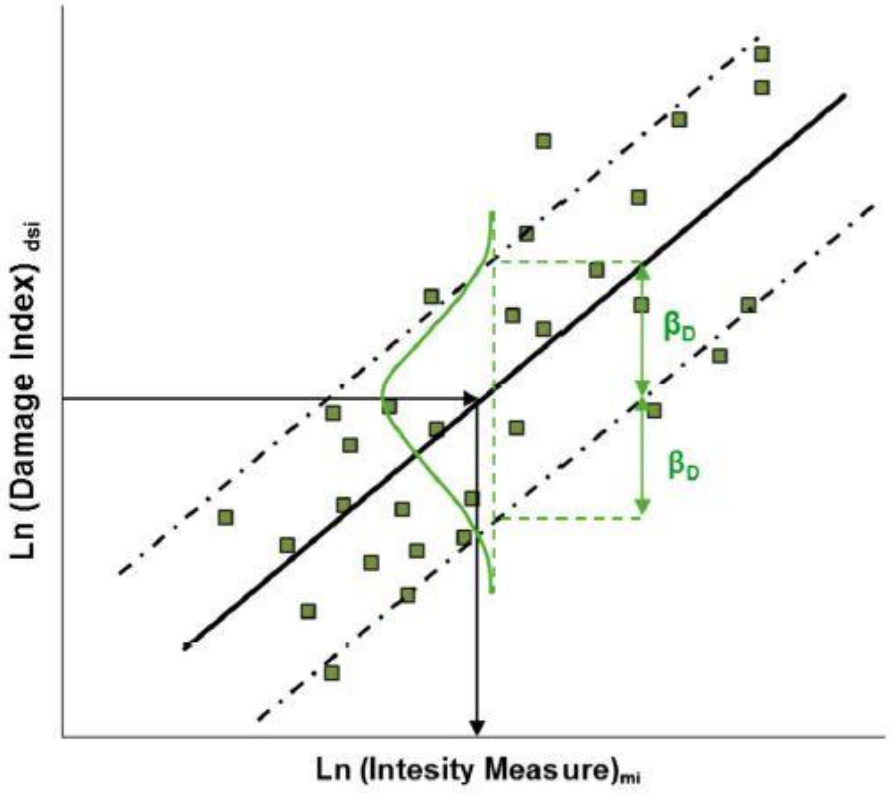

Fig. 3.5. Example of evolution of damage with earthquake intensity measure (S)-definition of threshold median value (S_{mi}) for the damage state i (ds_i) and standard deviation (β_D) due to variability of input motion (demand) (Argyroudis & Kaynia, 2015)

Determination of S_{mi}

Using the results of numerical analysis, the computed damage indices versus earthquake intensity parameter PGA diagram may be plotted and a trend line may also be obtained. Using the equation of the trend line mean standard threshold value of earthquake intensity measure (i.e. S_{mi}) corresponding to all the considered damage states is determined.

After determining all the required parameters the probability of damage is calculated according to Eq. 3.12. Then the plot of probability of damage against seismic intensity (i.e. PGA) gives the seismic fragility curve for given damage state.

CHAPTER 4

INFLUENCE OF STRATIFICATION ON TUNNEL LINING

4.1 General

It has been observed that stratification of geological medium through which tunnel passes has an adverse impact on stability of tunnel supports during seismic events. In stratified rock mass seismic vulnerability increases due to stiffness and seismic impedance mismatch as it causes differential kinetic movement. In addition to this amplified ground motion further enhance forces in tunnel lining leading to its failure. The present chapter focuses on the effect of stratification on the seismic response of the tunnel lining system. Comparison has been made between the seismic response of tunnel liner in single layer and two layer geological set up in terms of shear force, axial force and bending moment.

4.2 Details of Tunnel System Considered

A circular tunnel of 5.0 m radius having a circular lining of thickness 200 mm located at a depth of 25 m below the ground surface is considered. Two types of systems are considered. In first case single layer system consisting of V grade rock is considered. In second case two layered rockmass system is considered. The upper stratum is 50 m thick consisting of V grade rock and the lower strata is 150 m thick which has IV grade rockmass. The tunnel is located in upper strata i.e. V grade rockmass. Rock mass properties are adopted from Shen *et al*. (2014) and are presented in Table 4.1. The properties of shotcrete liner are presented in Table 4.2.

4.3 Modeling in UDEC

Propagation of dynamic waves without significant distortion is very essential to get accurate results in dynamic analyses. Zone size, boundary conditions are also important parameters which influence the propagation of dynamic waves. Hence suitable boundary conditions for static and dynamic analysis as discussed in *Section 3.3.3* and *Section 3.3.4* respectively are provided. Moreover appropriate mesh size according to guidelines discussed in *Section 3.3.4* is adopted.

Table 4.1. Properties of rock mass considered for the study (Shen *et al.* 2014)

Property	**V grade rock and soil**	**IV grade rock mass**
Density (kg/m^3)	1850	2200
Bulk Modulus (GPa)	1.2	3.1
Poisson's ratio	0.4	0.3
Cohesion (kPa)	200	400
Internal friction angle (degree)	30	40

Table 4.2. Properties of shotcrete liner

Thickness of tunnel liner, t (m)	Moment of Inertia I (m^4/m)	Poisson's ratio of tunnel lining, ν	Concrete Strength σ_c(MPa)
0.2	0.000667	0.2	20-35

The UDEC mesh is shown in Fig.4.1. Finer mesh size of 2 m is adopted for the regions close to the tunnel. The mesh size is made coarser i.e. 5 m and 15 m for the remaining region away from the tunnel.

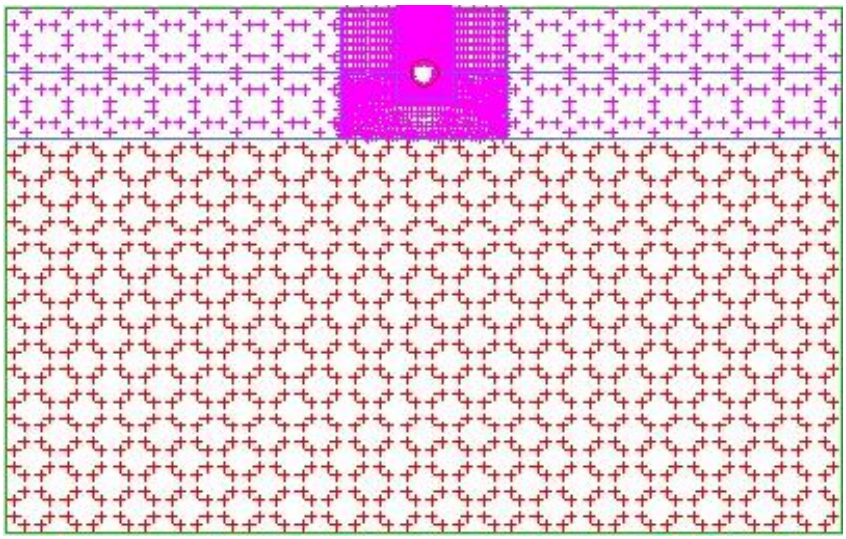

Fig. 4.1. View of the mesh in UDEC

4.4 Tunnel in Single Layer Deposit

In this section the tunnel is assumed to be in a single layer geologic strata of homogenous rock mass. Both static and dynamic analyses have been carried out for this system. Model configuration adopted for the numerical simulation is discussed in following sections.

4.4.1 Static Analysis

The model considered for static analysis is shown in Fig. 4.2. Left and right boundaries are placed on rollers in order to restrict movement in horizontal direction. Bottom boundary is also placed on roller to restrict displacement in vertical direction. Total thickness single layer rock mass is 200 m. The model is executed for 10,000 cycles to make the unbalanced forces insignificant and stable.

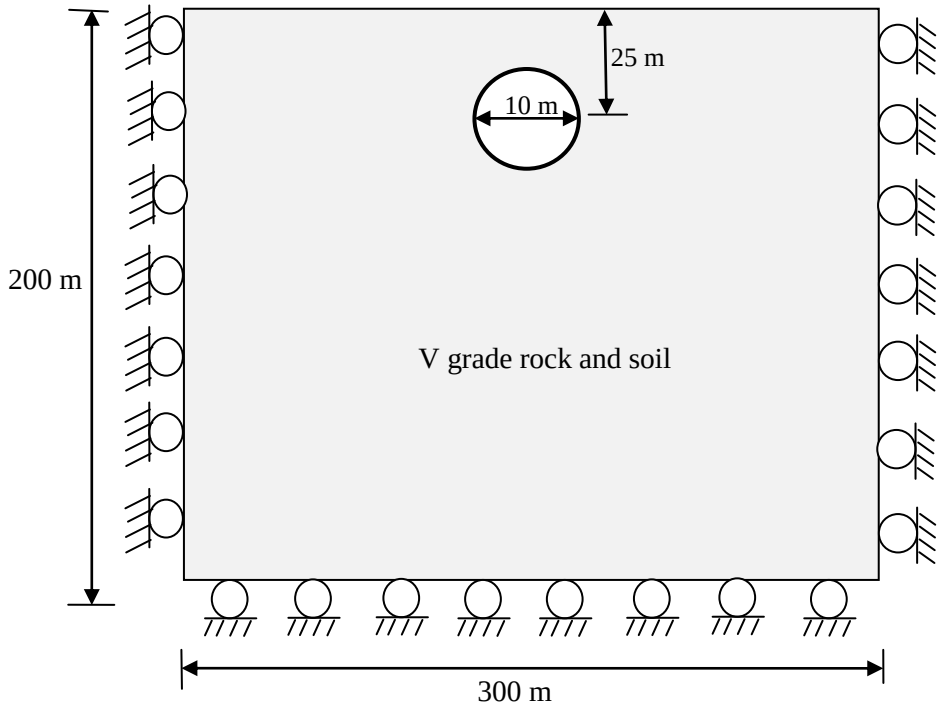

Fig. 4.2. Schematic of tunnel in single layer deposit for static analysis

4.4.2 Dynamic Analysis

The dynamic input is applied in form of stress history input (SHI) at the base of the model. Viscous dashpots are provided at bottom which absorbs incoming waves. In order to minimize the wave reflection from artificial boundaries free field boundary conditions are provided on left

and right boundaries of the model. Analysis is run for sufficient duration based on the duration of input motion. Fig. 4.3 shows the schematic of the model considered for dynamic analysis.

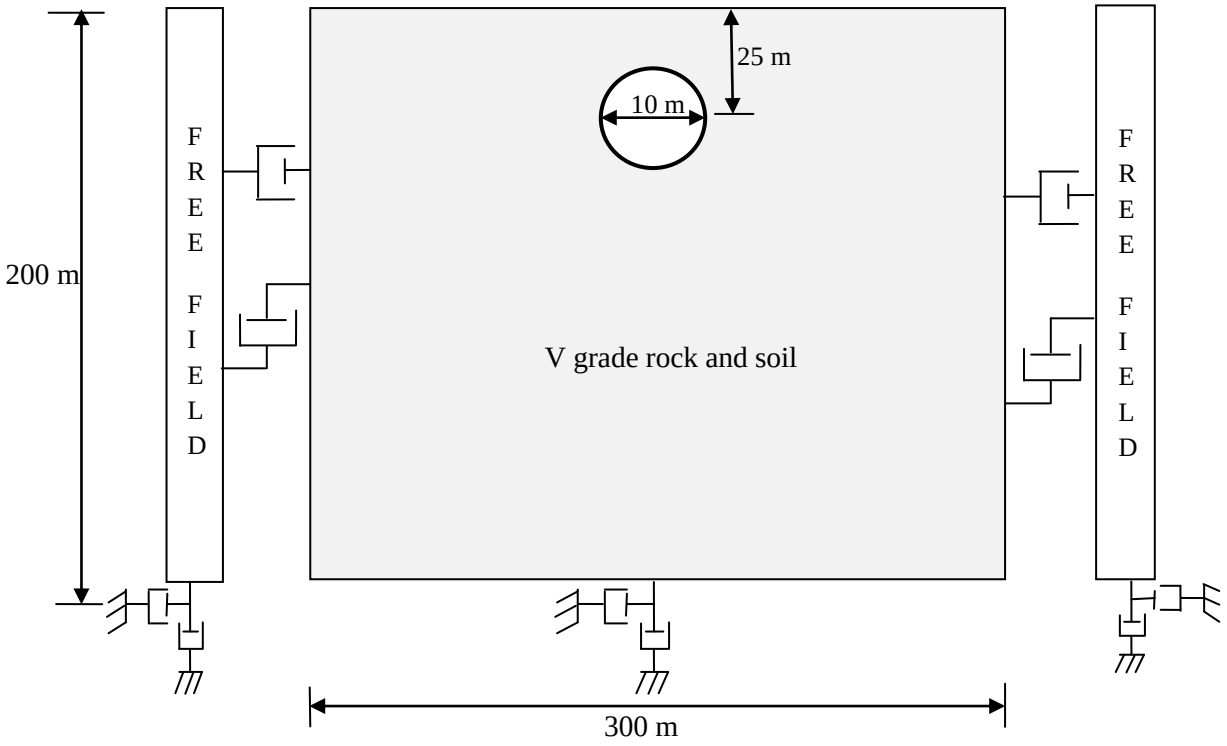

Fig. 4.3. Schematic of tunnel in single layer deposit for dynamic analysis

4.5 Tunnel in Stratified Deposit

In order to evaluate the impact of stratification on the performance of tunnel supports under dynamic condition, static and dynamic analysis of a two layered system is performed. Model configuration adopted for the numerical simulation is represented in following sections.

4.5.1 Static Analysis

The model for static analysis is shown in Fig.4. 4. A 50 m thick soft rock is underlain by 150 m thick hard rock. Left and right boundaries are placed on rollers in order to restrict movement in horizontal direction. Bottom boundary is also placed on roller to restrict displacement in vertical direction. The model is executed for 10,000 cycles to make the system unbalanced forces insignificant and stable.

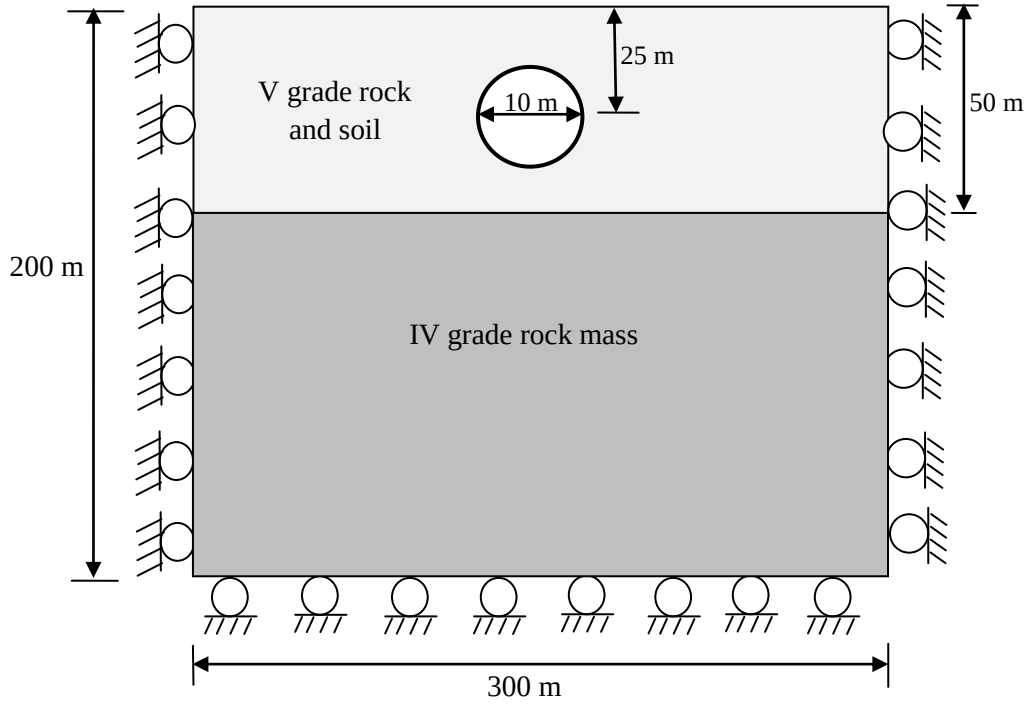

Fig. 4.4. Schematic of tunnel in stratified deposit for static analysis

4.5.2 Dynamic Analysis

Similar to single layer case, the dynamic input is applied in form of stress history input (SHI) at the base of the model. Viscous dashpots are provided at bottom which absorbs incoming waves. In order to minimize the wave reflection from artificial boundaries free field boundary conditions are provided on left and right boundaries of the model. Analysis is run for sufficient duration based on the duration of input motion. Fig. 4.5 shows the model considered for dynamic analysis.

4.6 Comparative Study for Tunnel in Single Layer and Stratified Deposit

The models discussed above are subjected to two types of loading. A sinusoidal wave for 20 cycles with frequencies of 2.0 Hz, 2.5 Hz, 3.0 Hz, 5.0 Hz and 10.0 Hz are applied. The maximum value of axial force, shear force and bending moment in tunnel liner is determined for both the cases. Similarly forces and moments are evaluated for real earthquake time histories of Coyote, Kobe, Kocaeli, Mammoth Lake, Northridge, Parkfield, Whitter Narrows earthquakes. The grade of concrete of shotcrete liner used is 20 MPa.

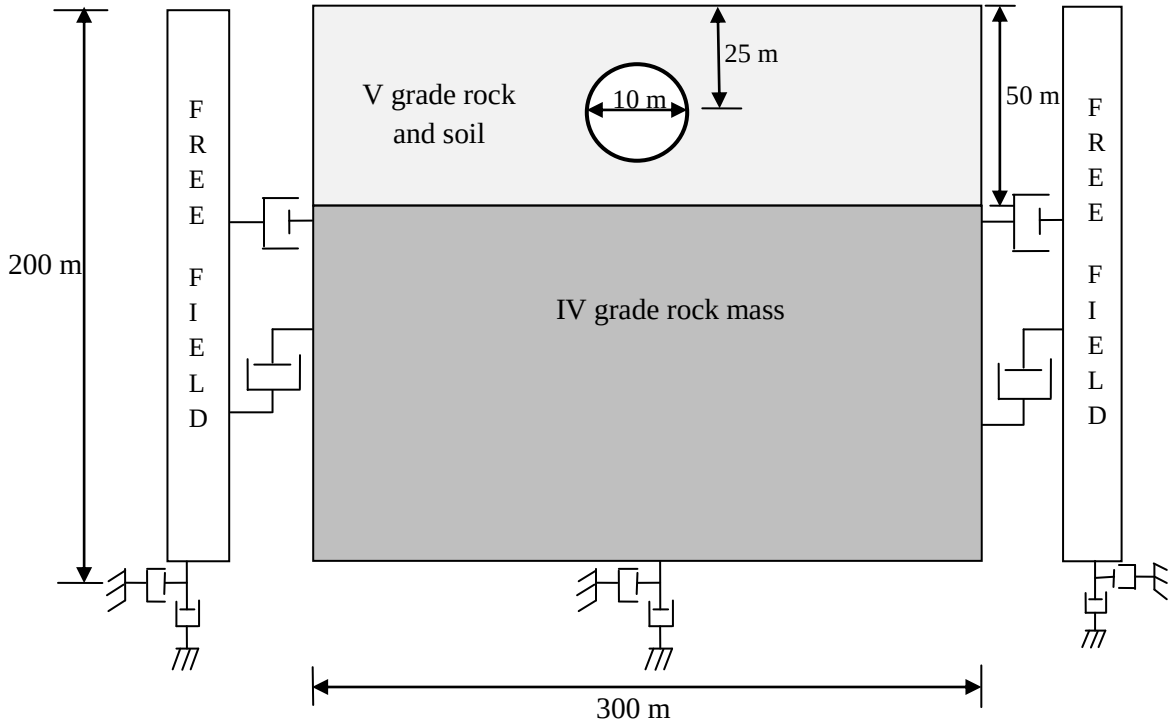

Fig. 4.5. Schematic of tunnel in stratified deposit for dynamic analysis

4.6.1 Axial Forces in Tunnel Liner

Axial forces in liner for both cases *i.e.* tunnel located in homogenous rock mass and stratified rock mass are evaluated. Fig. 4.6 compares the results for excitation with sinusoidal harmonic waves whereas Fig. 4.7 shows the comparison for earthquake time histories. It can be observed that axial forces in tunnel lining are more in case of stratified deposit.

4.6.2 Shear Forces in Tunnel Liner

Fig. 4.8 compares the results for sinusoidal harmonic waves whereas Fig. 4.9 presents the comparison for earthquake time histories. It has been observed that shear forces in tunnel liner are more in case of stratified deposit.

4.6.3 Bending Moments in Tunnel Liner

Fig. 4.10 compares the bending moments for a sinusoidal harmonic excitations whereas Fig. 4.11 shows a comparison for earthquake time histories. It may be observed that the bending moments in tunnel liner are more in case of two layer system.

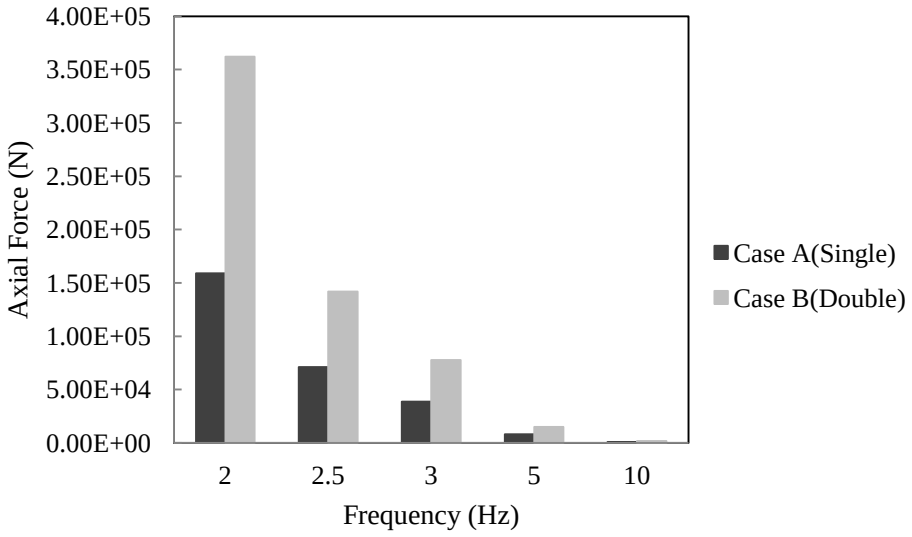

Fig. 4.6. Comparison of axial forces in tunnel liner for harmonic excitations

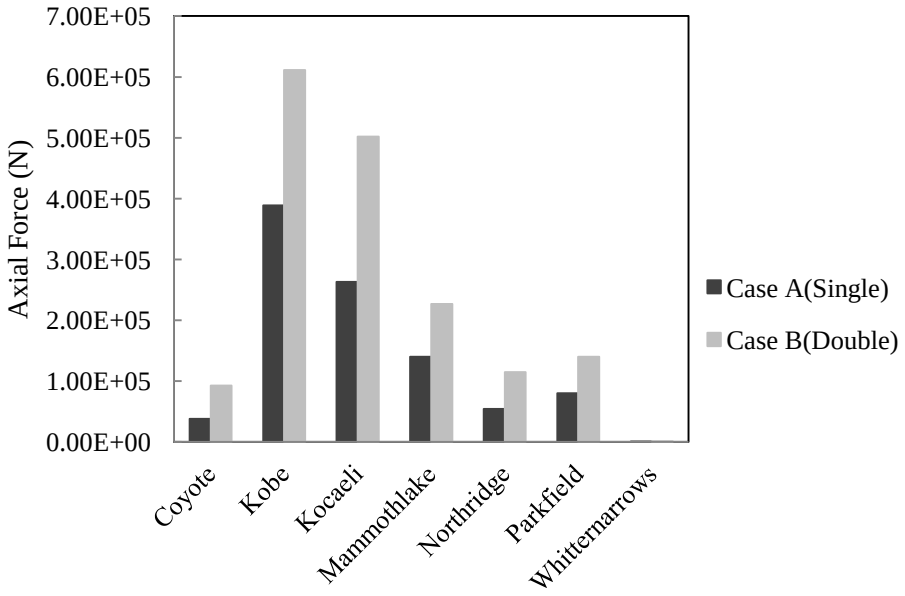

Fig. 4.7. Comparison of axial forces in tunnel liner for earthquake time histories

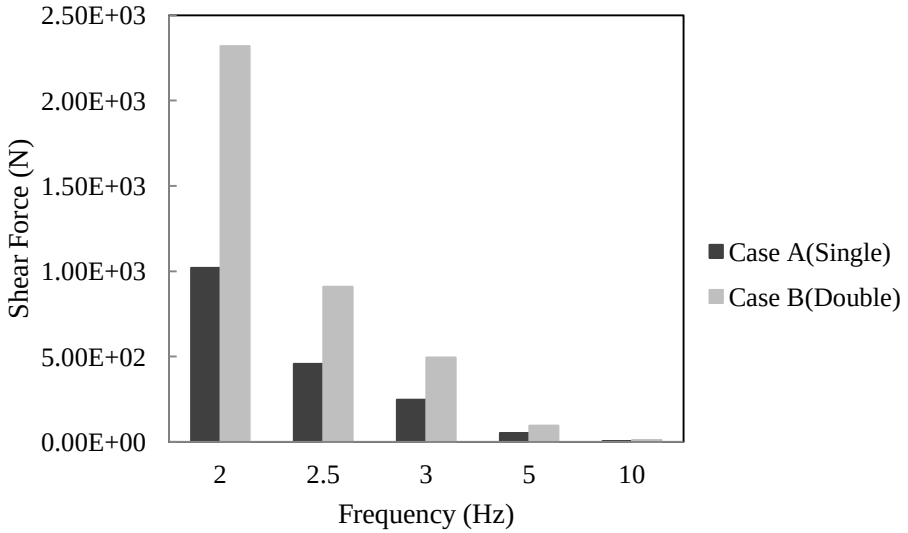

Fig. 4.8. Comparison of shear forces in tunnel liner for harmonic excitations

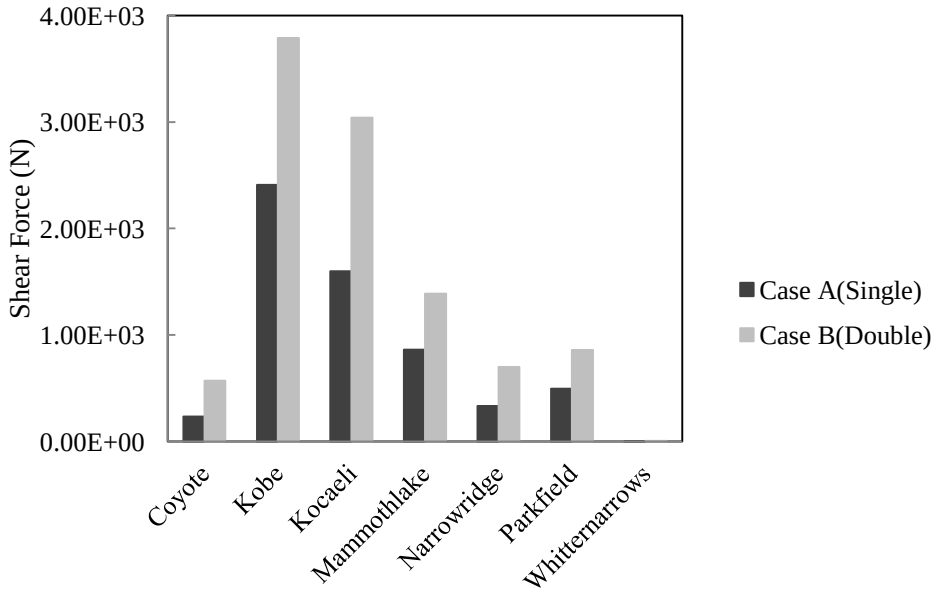

Fig. 4.9. Comparison of shear forces in tunnel liner for earthquake time histories

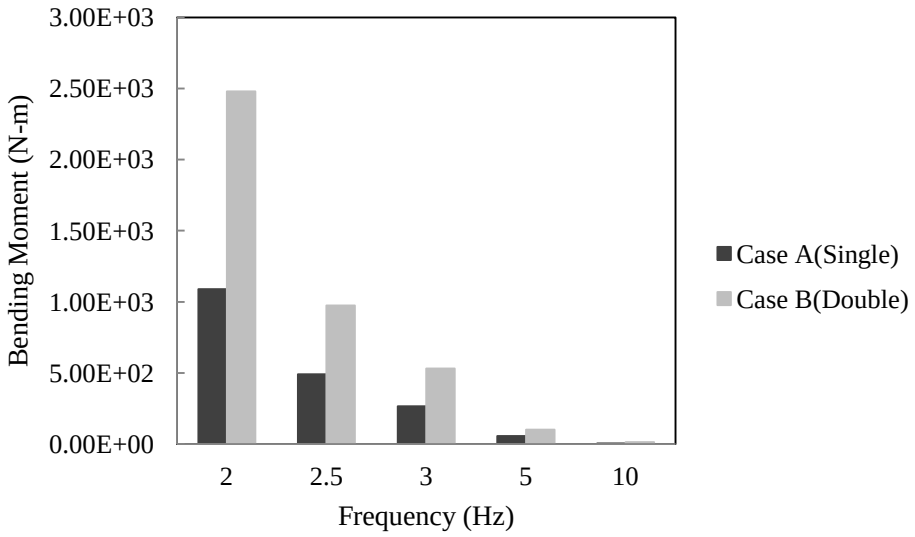

Fig. 4.10. Comparison of bending moment in tunnel liner for harmonic excitations

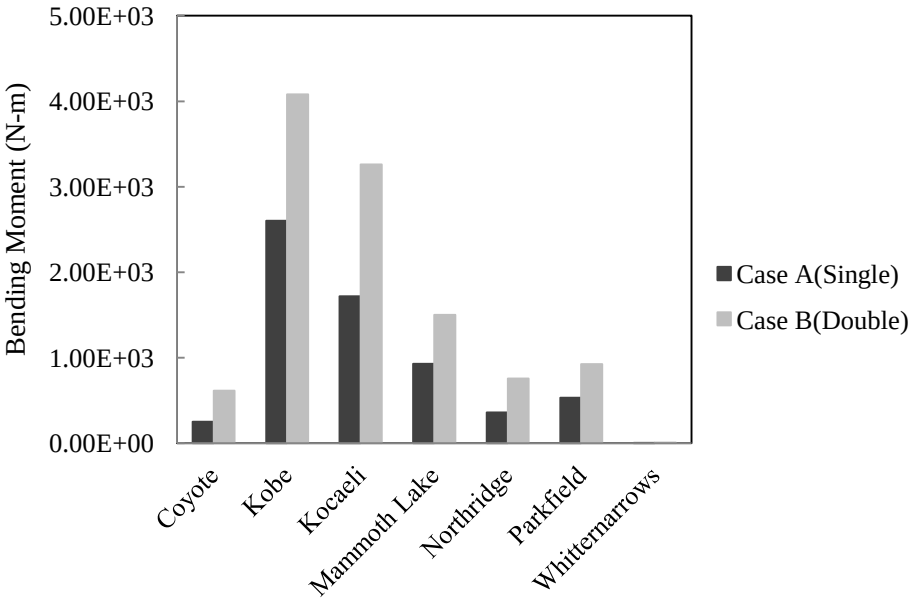

Fig. 4.11. Comparison of bending moment in tunnel liner for earthquake time histories

4.7 Concluding Remarks

From the above analysis it is be concluded that during seismic events tunnel support (liner in this study) is more vulnerable when tunnel is located in stratified deposits. The reason of this high vulnerability of liner is the stiffness and seismic impedance mismatch between different strata in stratified medium which leads to differential kinetic movement.

CHAPTER 5

GENERATION OF SEISMIC FRAGILITY CURVES FOR TUNNEL SUPPORTS

5.1 General

As concluded in chapter 4 tunnel supports being more vulnerable when tunnel passes through stratified medium hence the seismic fragility curves are derived for tunnel liner when the tunnel is located in two layered stratified geologic set up. For this purpose, the dynamic analyses have been performed on the system described in *Section 4.5.2*. The PGA is taken as earthquake input motion parameter and axial stress in shotcrete liner is selected as representative damage indicator.

Behavior of tunnel liner is modeled with elastic beam elements and for estimating the actual forces two types of loading are considered. In first case, analysis is run for a sinusoidal harmonic excitations and in second case seven real earthquake time histories are considered. From the maximum value of axial force in the liner, the maximum stresses are estimated. The capacity of the tunnel support is calculated based on the grade of concrete, thickness of liner and geometry of tunnel represented by Eq. 5.1 (Oreste 2003).

$$\sigma_{\max,shot} = \frac{1}{2} \cdot \sigma_c \cdot \left[1 - \frac{(R - t_{shot})^2}{R^2} \right] \tag{5.1}$$

where $\sigma_{max,shot}$ is the maximum permissible stress in shotcrete lining; σ_c is the compressive strength of concrete; R is the radius of tunnel and t_{shot} is the thickness of the shotcrete liner.

Maximum obtained axial stress is then compared with permissible stress i.e. capacity of shotcrete liner. The level of tunnel damage is described by damage index which is the ratio of induced stresses in shotcrete liner to its strength capacity. Based on the damage index six different damage states as represented in Table 3.2 is considered. The probability of reaching or exceeding a particular damage state is expressed by a lognormal probability distribution provided by Eq. (3.12).

5.2 Fragility Curves with Harmonic Excitations

Harmonic sinusoidal waves with 20 cycles and frequencies 2.0 Hz, 2.5 Hz, 3.0 Hz, 5.0 Hz and 10.0 Hz are applied at the base of the model. The peak amplitude of wave is varied from 0.02g to 1.50g at an interval of 0.05g. A typical wave for frequency 2 Hz and peak amplitude of acceleration 0.2g is shown in Fig. 5.1. The grade of concrete of shotcrete liner is taken as M20 and thickness of lining is 200mm. Model is executed for sufficient duration based on the time duration of the sinusoidal wave motion. Maximum value of axial force in the liner is recorded. A typical plot of axial force in liner with time as recorded from UDEC for frequency 2.0 Hz and peak amplitude of acceleration 0.2g is shown in Fig. 5.2. It may be observed that the maximum axial force mobilized in the tunnel support section is 72.5 kN. However, with an increase in the PGA of the sinusoidal wave fed into the system, the axial force increases. Fig. 5.3 shows the axial force in the tunnel liner when the PGA is 1.0g. In this case, the maximum value of axial force is 362 kN.

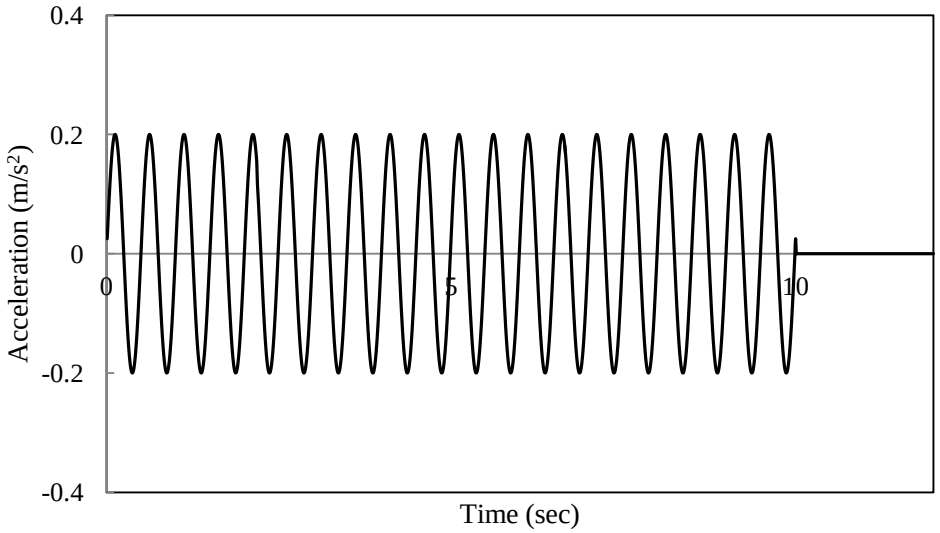

Fig. 5.1. Typical incident harmonic excitation (PGA 0.2g; Frequency 2Hz)

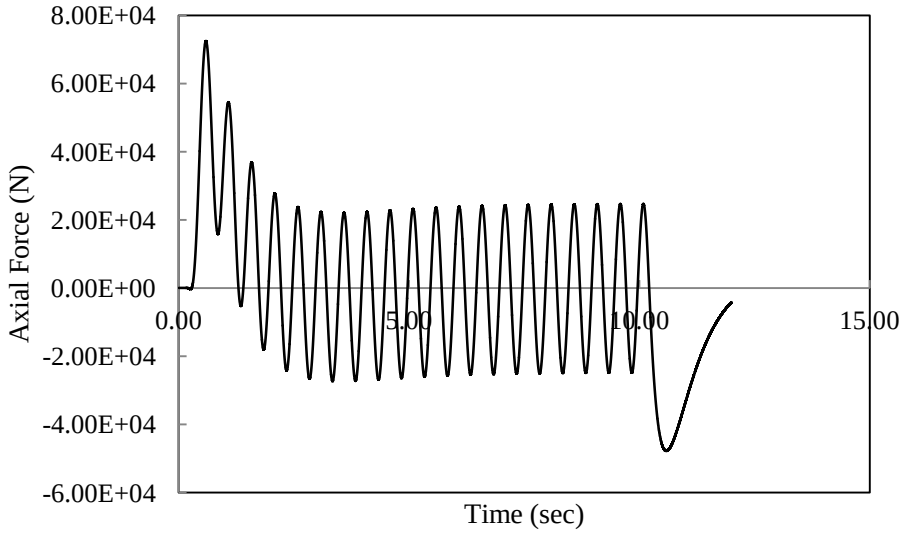

Fig. 5.2. Axial force in tunnel liner for harmonic excitation (PGA 0.2g; Frequency 2Hz)

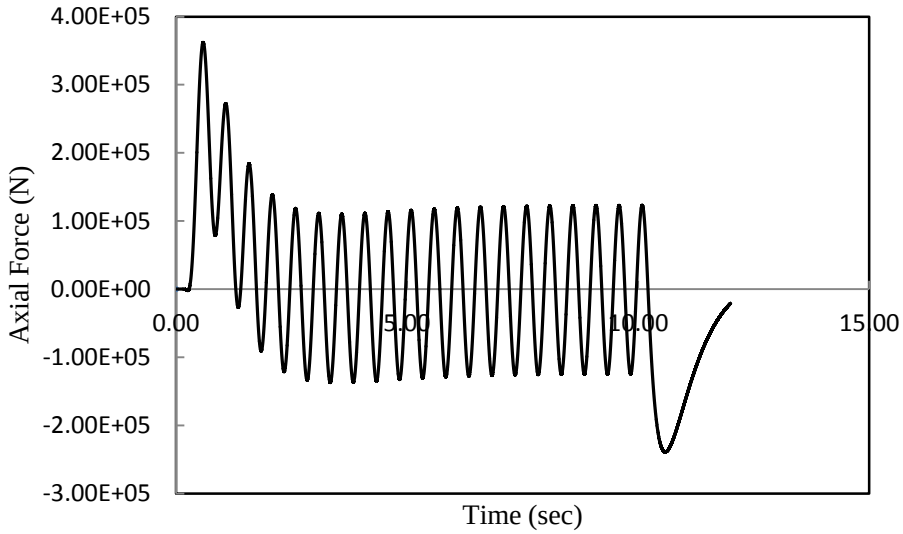

Fig. 5.3. Axial force in tunnel liner for harmonic excitation (PGA 1.0g; Frequency 2Hz)

Based on the axial force, axial stresses are obtained by dividing the force with area of liner of unit length i.e. 200000 mm^2. The maximum permissible value of stress in shotcrete $\sigma_{max,shot}$ for M20 grade of concrete of shotcrete is calculated based on Eq. 5.1 and comes out to be 0.784 MPa. The ratio of induced stresses in the liner to the capacity gives the damage index. For

estimating β_{tot} the value of β_D is obtained by the procedure described in *Section 3.4.3* and is obtained as 2.39. Hence the value of β_{tot} is calculated as 2.44.

Further for estimating S_{mi}, computed damage index versus earthquake intensity (*i.e.* PGA) is plotted for all the five frequencies (i.e. 2.0 Hz, 2.5 Hz, 3.0 Hz, 5.0 Hz and 10.0 Hz) as shown in Fig. 5.4. Based the trend line obtained from graph, S_{mi} is evaluated for all the six damage states and is represented in Table 5.1.

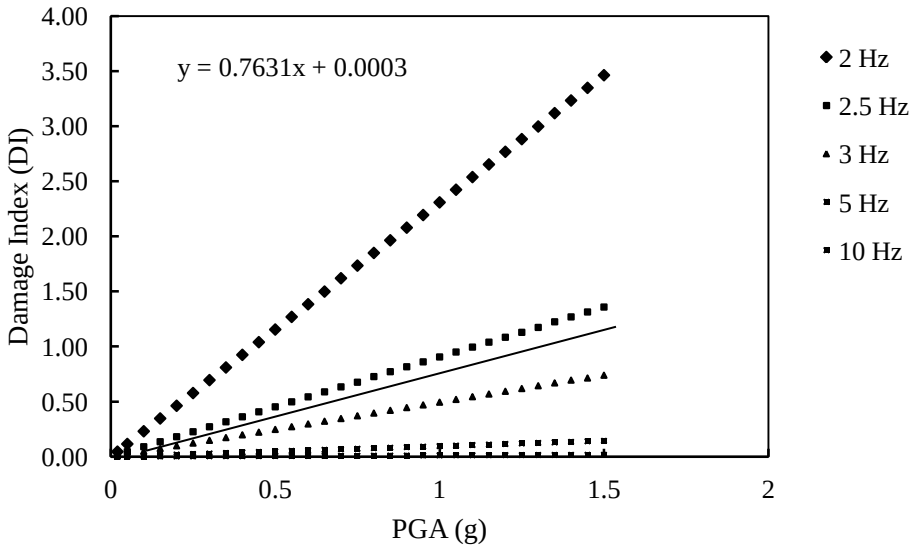

Fig. 5.4. Damage index (DI) with PGA for harmonic excitations (M20 grade of concrete)

Table 5.1. S_{mi} values corresponding to considered damage states for harmonic excitations

Sl. No.	Damage State (DS)	S_{mi}
1.	DS = 0.75	0.9824
2.	DS = 1.00	1.3101
3.	DS = 1.25	1.6377
4.	DS = 1.50	1.9653
5.	DS = 1.75	2.2929
6.	DS = 2.00	2.6205

The probability of damage for each of the damage state is evaluated using Eq. (3.12). The fragility curves *i.e.* plot of probability of damage against PGA for all the damage states are shown in Fig. 5.5.

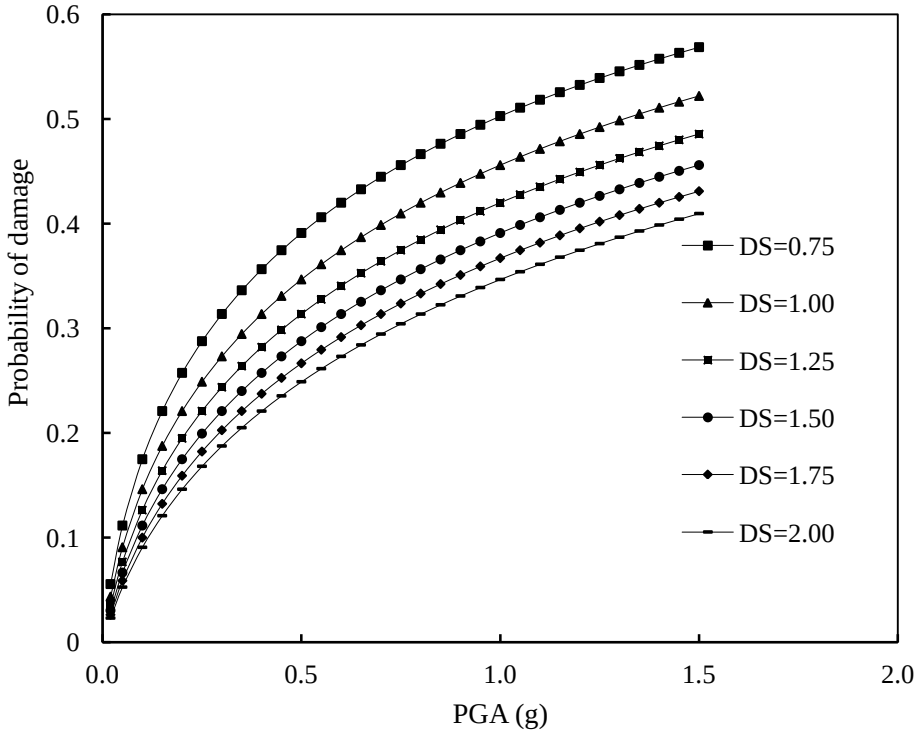

Fig. 5.5. Fragility curves for harmonic excitations (M20 grade shotcrete)

5.3 Fragility Curves with Earthquake Time Histories

Subsequently, the assessment of seismic fragility curves for the tunnel liner situated in the two layered rock mass system have been evaluated using real earthquake time histories. For this purpose, time histories of Coyote, Kobe, Kocaeli, Mammoth Lake, Northridge, Parkfield, Whitter Narrows earthquakes with predominant frequencies and time durations as shown in Table 5.2 are applied at the base of the model. Time history for Coyote earthquake is shown in Fig. 5.6. Each acceleration time history is normalized by dividing acceleration by absolute maximum acceleration (*i.e.* A/Amax). For Coyote earthquake normalized time history is shown in Fig. 5.7 which is obtained by dividing acceleration time history by A_{max} i.e. 0.124g. The time histories are then scaled from 0.10g to 1.00g at an interval of 0.15g.

Table 5.2. Earthquake time histories

Sl. No.	Time History	Dominant Frequency (Hz)	Duration (Sec)
1.	Coyote	2.39	26.835
2.	Kobe	1.45	48.00
3.	Kocaeli	5.35	30.00
4.	Mammoth Lake	2.41	29.955
5.	Northridge	5.01	40.00
6.	Parkfield	2.63	30.33
7.	Whitter Narrows	6.41	39.995

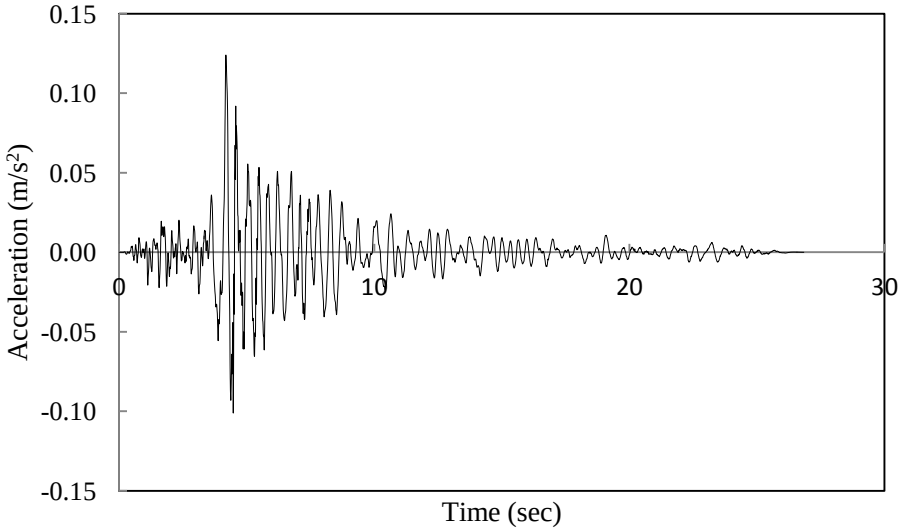

Fig. 5.6. Time history for Coyote earthquake

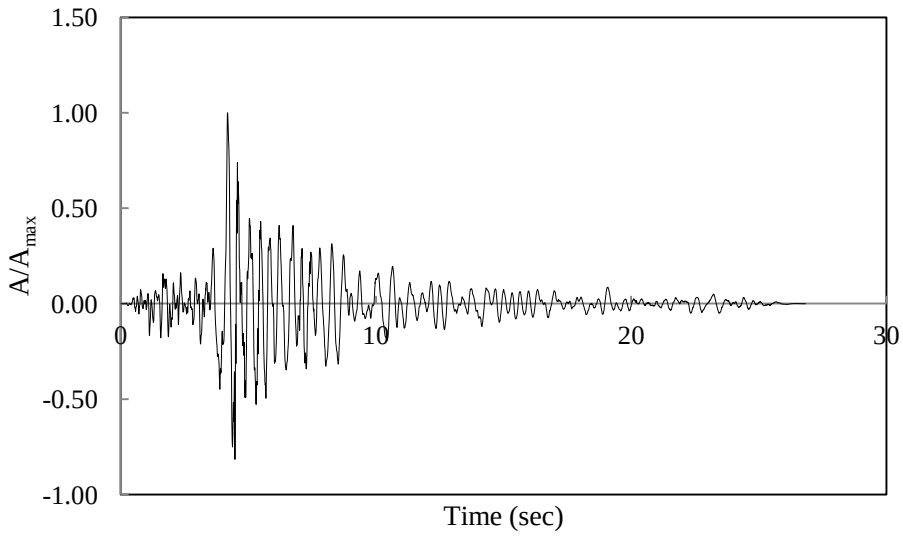

Fig. 5.7. Normalized time history for Coyote earthquake

The grade of concrete of shotcrete for the tunnel liner is considered to be M20, M25, M30 and M35 and the thickness of liner is considered as 200 mm. Model is executed for sufficient duration based on the duration of respective earthquake time history. Maximum value of axial force in the liner is recorded. Stresses are then obtained by dividing forces with area of liner of unit length *i.e.* 200000 mm^2.

5.3.1 For M20 Grade Shotcrete

The maximum permissible value of stress in shotcrete $\sigma_{max,shot}$ for M20 grade of shotcrete is calculated from Eq. 5.1 and comes out to be 0.784 MPa. Then the damage index *i.e.* ratio of induced stresses in the liner to capacity is obtained. For estimating β_{tot} the value of β_D is obtained by the procedure described in *Section 3.4.3* and is obtained as 2.13. Hence the value of β_{tot} is calculated as 2.18.

Further for estimating S_{mi} , computed damage index versus earthquake intensity (*i.e.* PGA) is plotted for all the seven time histories as shown in Fig. 5.8. From the trend line obtained from graph, S_{mi} is evaluated for all the six damage states and is presented in Table 5.3.

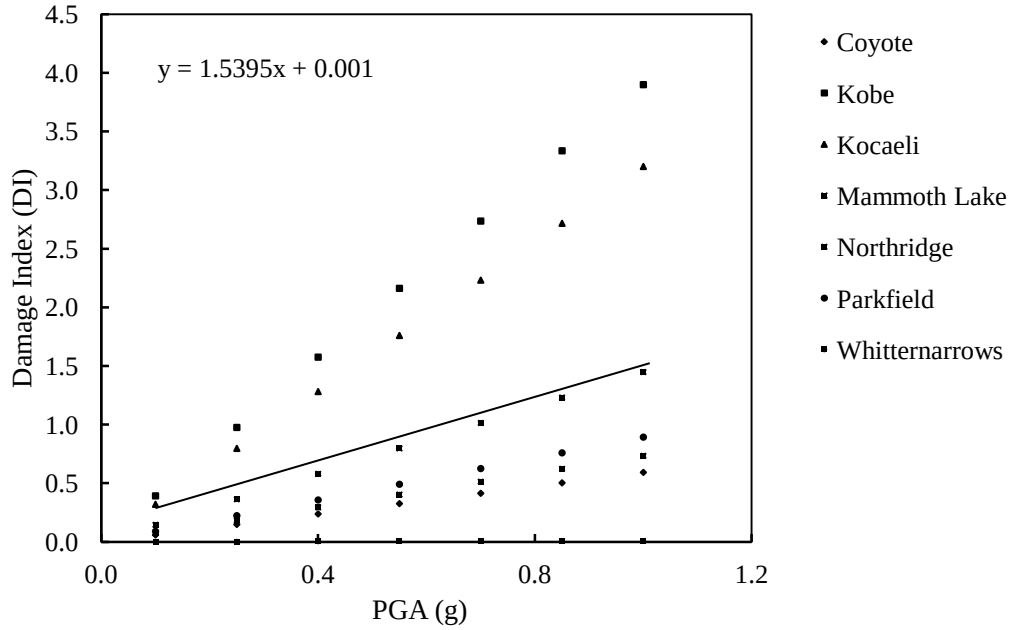

Fig. 5.8. Evolution of damage index (DI) for earthquake time histories (M20 grade shotcrete)

Table 5.3. S_{mi} values of damage states for earthquake time histories (M20 grade shotcrete)

Sl. No.	Damage State (DS)	S_{mi}
1.	DS = 0.75	0.4865
2.	DS = 1.00	0.6489
3.	DS = 1.25	0.8113
4.	DS = 1.50	0.9737
5.	DS = 1.75	1.1361
6.	DS = 2.00	1.2985

The probability of damage for each of the damage state is evaluated using Eq. 3.12. The fragility curves (*i.e.* plot of probability of damage against PGA) for all the damage states for M20 grade of concrete of shotcrete lining is shown in Fig. 5.9.

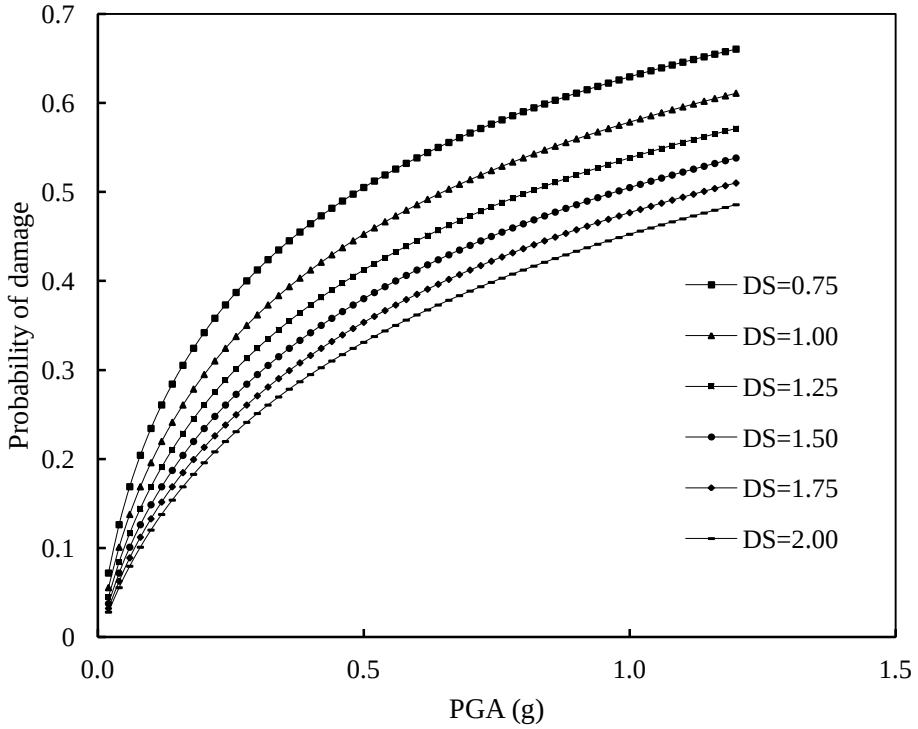

Fig. 5.9. Fragility curves for earthquake time histories (M20 grade shotcrete)

5.3.2 For M25 Grade Shotcrete

The maximum permissible value of stress in shotcrete $\sigma_{max,shot}$ for M25 grade shotcrete is calculated from Eq. 5.1 and comes out to be 0.980 MPa. As discussed in *Section 3.4.3*, β_{tot} and β_D are 2.13 and 2.183 respectively.

Further for estimating S_{mi} computed damage index versus earthquake intensity (*i.e.* PGA) is plotted for all the seven time histories as shown in Fig. 5.10. From the trend line obtained from graph, S_{mi} is evaluated for all the six damage states and is represented in Table 5.4.

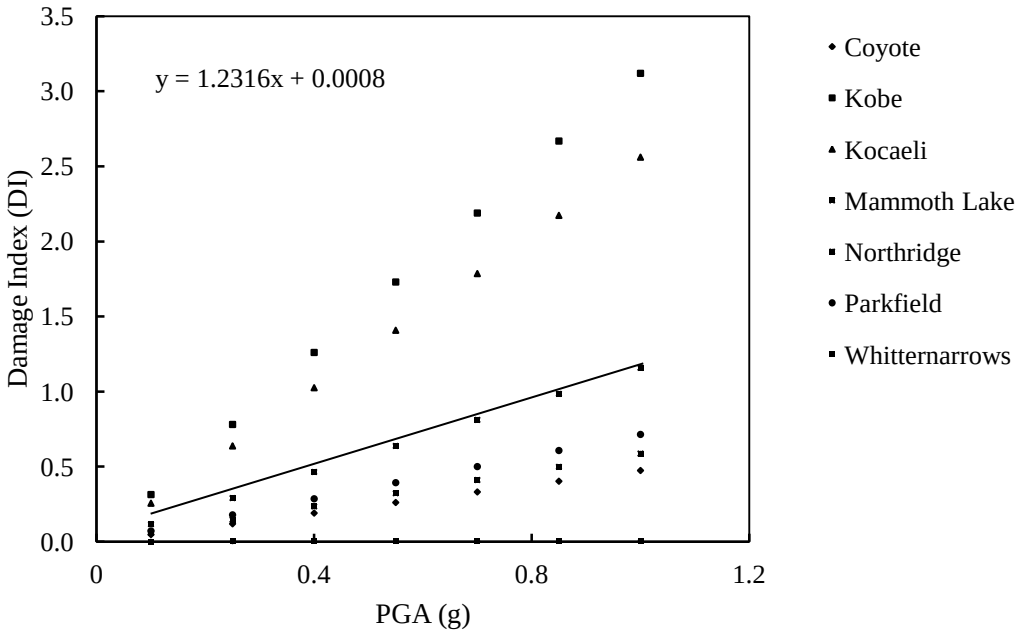

Fig. 5.10. Evolution of damage index (DI) for earthquake time histories (M25 grade shotcrete)

Table 5.4. S_{mi} values of damage states for earthquake time histories (M25 grade shotcrete)

Sl. No.	Damage State (DS)	S_{mi}
1.	DS = 0.75	0.6083
2.	DS = 1.00	0.8113
3.	DS = 1.25	1.0143
4.	DS = 1.50	1.2173
5.	DS = 1.75	1.4203
6.	DS = 2.00	1.6233

The probability of damage for each of the damage states is evaluated using Eq. 3.12. The fragility curves (i.e. plot of probability of damage against PGA) for all the damage states for M25 grade of concrete of shotcrete are shown in Fig. 5.11.

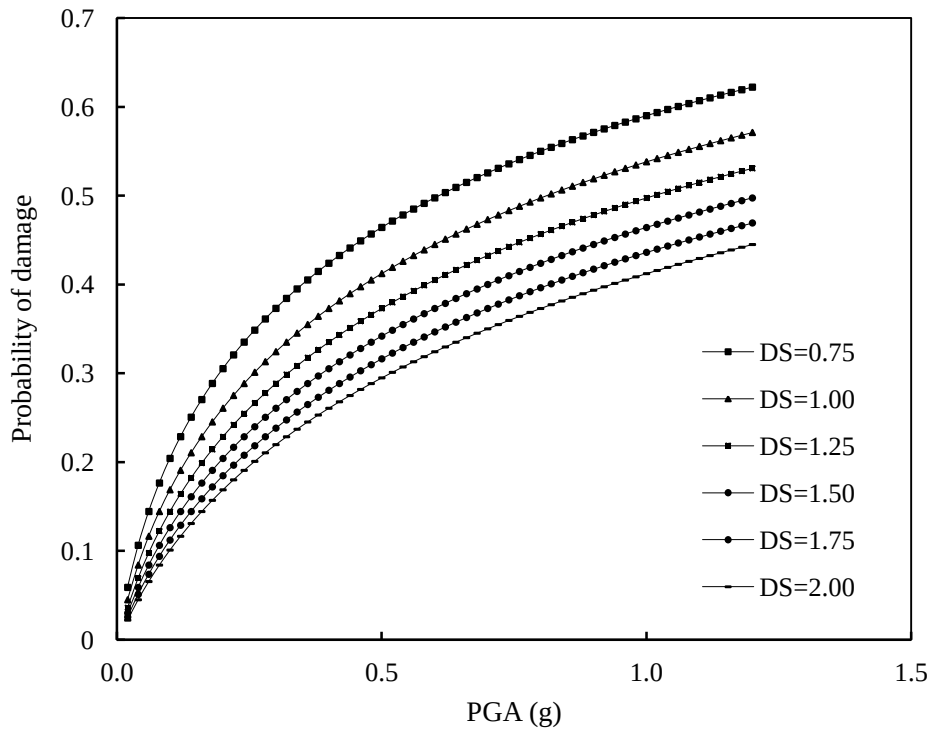

Fig. 5.11. Fragility curves for earthquake time histories (M25 grade shotcrete)

5.3.3 For M30 Grade Shotcrete

The maximum permissible value of stress in shotcrete $\sigma_{max,shot}$ for M30 grade of concrete of shotcrete is calculated from Eq. 5.1 and comes out to be 1.176 MPa.

Further for estimating S_{mi} computed damage index versus earthquake intensity (i.e. PGA) is plotted for all the seven time histories as shown in Fig. 5.12. From the trend line obtained from graph, S_{mi} is evaluated for all the six damage states and is represented in Table 5.5.

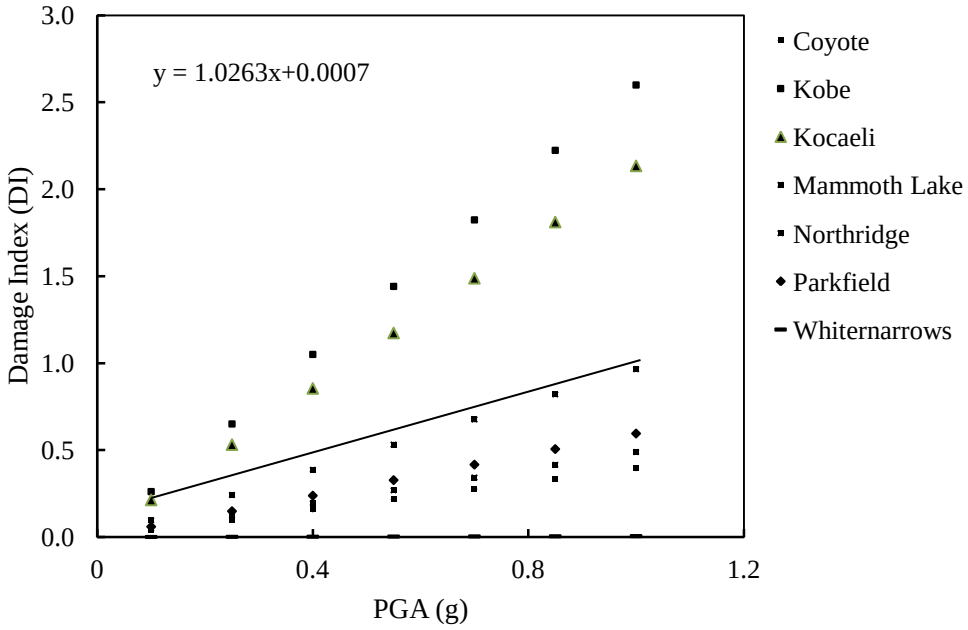

Fig. 5.12. Evolution of damage index (DI) for earthquake time histories (M30 grade shotcrete)

Table 5.5. S_{mi} values of damage states for earthquake time histories (M30 grade shotcrete)

Sl. No.	Damage State (DS)	S_{mi}
1.	DS = 0.75	0.7301
2.	DS = 1.00	0.9737
3.	DS = 1.25	1.2173
4.	DS = 1.50	1.4609
5.	DS = 1.75	1.7045
6.	DS = 2.00	1.9481

The probability of damage for each of the damage state is evaluated using Eq. 3.12. The fragility curves (*i.e.* plot of probability of damage against PGA) for all the damage states for M30 grade of concrete of shotcrete are shown in Fig. 5.13.

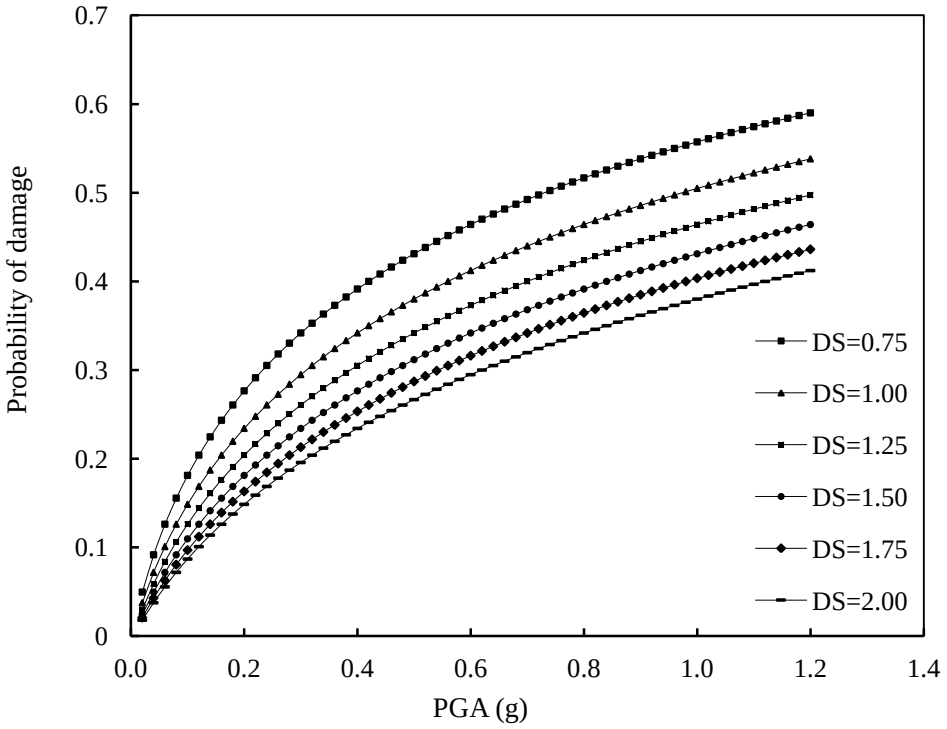

Fig. 5.13. Fragility curves for earthquake time histories (M30 grade shotcrete)

5.3.4 For M35 Grade Shotcrete

The maximum permissible value of stress in shotcrete $\sigma_{max,shot}$ for M35 grade shotcrete is calculated from Eq. 5.1 and comes out to be 1.715 MPa.

Further for estimating S_{mi} computed damage index versus earthquake intensity (*i.e.* PGA) is plotted for all the seven time histories as shown in Fig. 5.14. From the trend line obtained from graph, S_{mi} is evaluated for all the six damage states and is represented in Table 5.6.

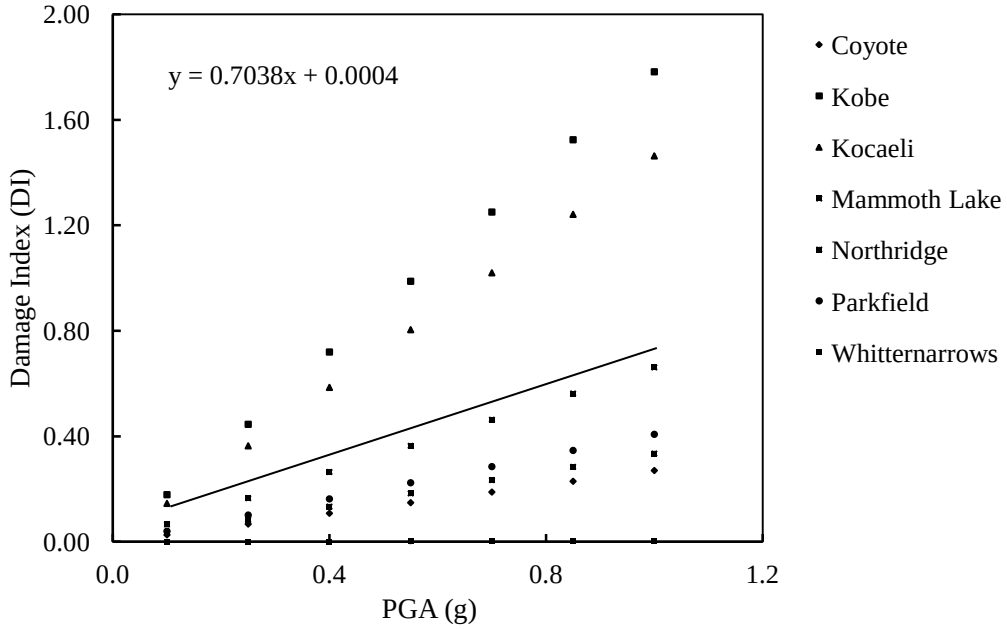

Fig. 5.14. Evolution of damage index (DI) for earthquake time histories (M35 grade shotcrete)

Table 5.6. S_{mi} values of damage states for earthquake time histories (M35 grade shotcrete)

Sl. No.	Damage State (DS)	S_{mi}
1.	DS = 0.75	1.0651
2.	DS = 1.00	1.4203
3.	DS = 1.25	1.7755
4.	DS = 1.50	2.1307
5.	DS = 1.75	2.4859
6.	DS = 2.00	2.8411

The probability of damage for each of the damage state is evaluated using Eq. 3.12. The fragility curves (*i.e*. plot of probability of damage against PGA) for all the damage states for M35 grade of concrete of shotcrete are shown in Fig.5.15.

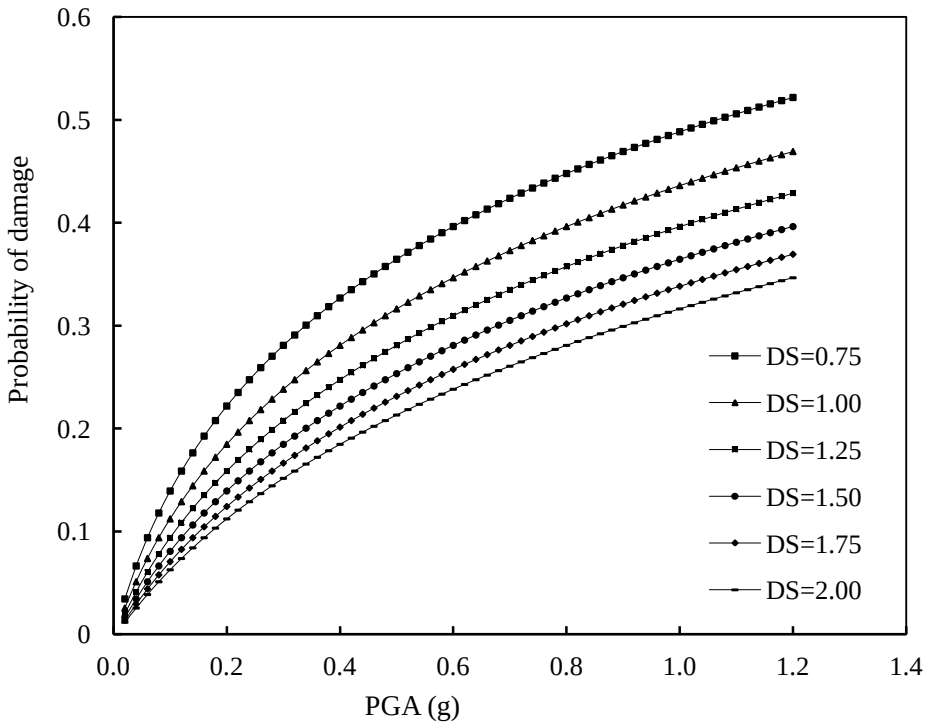

Fig. 5.15. Fragility curves for earthquake time histories (M35 grade shotcrete)

5.4 Application of Derived Fragility Curves

Fragility curves are used for understanding the response of structure to seismic events, risk assessment and risk management (expectation of losses and development of strategies to limit the extent of loss or damage caused by earthquake). Although fragility curves are specific to particular structural system but are flexible in use, hence they can be adapted to any region for similar structures and ground conditions.

5.5 Discussion and Conclusions

From the above derived fragility curves it can be observed that probability of damage, for a particular damage state, increases with an increase in PGA. Also probability of damage is less for higher damage state as for reaching or exceeding a high damage state it demands high level of earthquake intensity. The fragility curves are showing steep rise at low value of PGA. The similar trend has also been presented by Rota *et al.* (2000) while deriving fragility curves for Italian structures. This is partly due to selected analytical function *i.e.* lognormal distribution

function. Again at very low PGA fragility curves for all damage state have almost similar value of probability of damage.

Comparing fragility curves plotted for different grades *i.e.* M20, M25, M30 and M35 it can also be observed that probability of failure decreases with increasing grade of concrete of shotcrete liner due to an increase in capacity of liner. Thus for a constant demand (*i.e.* earthquake intensity) damage index will be less for higher grade of concrete. Subsequently the probability of damage for higher grade of concrete will also be less.

CHAPTER 6
SUMMARY AND DISCUSSIONS

6.1 Summary & Discussions

The increasing demand of infrastructure necessitates increasing tunneling activities. Mountain tunnels passes through wide variety of geological settings. The assessment of vulnerability in changing geological strata is of great importance.

In this thesis, the basic methodology followed in distinct element based software package UDEC has been discussed. Different modeling aspects in static and dynamic problems has been identified and discussed with sufficient details. From the analysis performed with UDEC it has been observed that in stratified deposits the amplified ground motion increase vulnerability of tunnel support system. The stiffness and impedance mismatch also been the key elements of increased vulnerability.

Fragility curves have been plotted for different damage states. It can be observed that probability of failure decreases for higher damage state as for reaching or exceeding a high damage state it demands high level of earthquake intensity. Fragility curves have also been derived for varying grades of concrete. It can be concluded that increasing the capacity of tunnel liner in terms of increased grade of concrete of shotcrete liner decreases the probability of damage of tunnel liner.

6.2 Future Recommendations

Based on the observations made in this study the recommendations are-

- The idealized model without considering discontinuities leads to underestimation of the forces in tunnel support system. Analysis should be performed with incorporating discontinuities in the system used.
- For deriving fragility curves using numerical method cumulative lognormal distribution function is mostly used, however other analytical expressions should also be reviewed for their suitability.

References

1. Argyroudis, S., and Kaynia, A.M., (2015). "Analytical seismic fragility functions for highway and railway embankments and cuts." *Earthquake Engineering & Structural Dynamics*. DOI: 10.1002/eqe.2563.
2. Argyroudis, S.A., and Pitilakis, K.D., (2012). "Seismic fragility curves of shallow tunnels in alluvial deposits." *Soil Dynamics and Earthquake Engineering*, 35, pp 1-12.
3. Asakura, T., Tsukada, K., Mastsunaga, T., Matsuoka, S., Yashiro, K., Shiba, Y., and Oya, T., (2000). "Damage to Mountain Tunnels by Earthquake and its Mechanism."
4. Cai, J.G. and Zhao, J. (2000). "Effects of multiple parallel fractures on apparent attenuation of stress waves in rock masses." *International Journal of Rock Mechanics and Mining Sciences*, 37 (2000), pp 661-682.
5. Cundall, P.A. (1971). A computer model for simulating progressive, large scale movement in blocky rock system." *Symp., ISRM, Nancy, France*, pp 129-136.
6. Erberik, M.A., (2008). "Generation of Fragility Curves for Turkish Masonry Buildings Considering in-Plane Failure Modes." *Earthquake Engineering & Structural Dynamics*, 34(3), pp 387-405.
7. Goodman, R.E., Taylor, R.L. and Brekke, T.L. (1968). "A model for the mechanics of the jointed rock." *Journal of the Soil Mechanics and Foundations Division, ASCE*, SM3, pp 637-695.
8. Ioannou, I. and Rossetto T. (2014). "Empirical Fragility." *Encyclopedia of Earthquake Engineering.* DOI 10.1007/978-3-642-36197-5_249-1. Springer-Verlag Berlin Heidelberg 2014.
9. Itasca *Inc.* (2004). UDEC user's manual. Minneapolis: Itasca Consulting Group Inc.
10. Jing, L. (2003). "A review of techniques, advances and outstanding issues in numerical modelling for rock mechanics and rock engineering." *International Journal of Rock Mechanics and Mining Sciences*, 40, pp 283-353.
11. Kaynia, A.M., (2013). Guidelines for deriving seismic fragility functions of elements at risk: Buildings, lifelines, transportation networks and critical facilities. *SYNGER-G Reference Report 4*.

12. King, S. A., Kiremidjian, A. S., Pachaki, D., and Sarabandi, P., (2004). "Application of Empirical Fragility Functions from Recent Earthquakes." *13th World Conference on Earthquake Engineering,* Vancouver, B.C., Canada, August 1-6, 2004, Paper No. 2829.

13. Lysmer, J. and Kuhlemeyer, R. (1989). "Finite Dynamic Model for Infinite Media." *Journal of Engineering Mechanics, (ASCE)* 95:EM4, 859-877.

14. Mayoral, J.M., Argyroudis, S., and Castañon, E., (2016). "Vulnerability of floating tunnel shafts for increasing earthquake loading." *Soil Dynamics and Earthquake Engineering,* 80, pp 1-10.

15. Oreste, P.P., 2003. "Analysis of structural interaction in tunnels using the convergence-confinement approach." Tunnelling and Underground Space Technology 18, pp 347–363.

16. Rota, M., Penna, A., and Strobbia, C.L., (2008). "Processing Italian damage data to derive typological fragility curves." *Soil Dynamics and Earthquake Engineering,* 28, pp 933–947.

17. Rota, M., Penna, A., Strobbia, C., and Magenes, G., (2008). "Direct Derivation of Fragility Curves from Italian Post-Earthquake Survey Data." *The 14th World Conference on Earthquake Engineering*, October 12-17, 2008, Beijing, China.

18. Sarbandi, P., Pachakis, P., King, S., and Kiremidjian, A., (2004). "Empirical Fragility Functions from Recent Earthquakes." *13th World Conference on Earthquake Engineering,* Vancouver, B.C., Canada, August 1-6, 2004, Paper No. 1211.

19. Shen, Y., Gao, B., Yang, X., and Tao, S., (2014). "Seismic damage mechanism and dynamic deformation characteristic analysis of mountain tunnel after Wenchuan earthquake." *Engineering Geology,* 180, pp. 85-98.

20. Shimizu, M., Suzuki, T., Kato, S., Kojima, Y., Yashiro, K., and Asakura, T., (2007). "Historical damages of tunnels in Japan and case studies of damaged railway tunnels in the Mid Niigata Prefecture Earthquakes." *Underground Space – the 4th Dimension of Metropolises – Barták, Hrdina, Romancov & Zlámal (eds).* Taylor & Francis Group, London, ISBN 978-0-415-40807-3.

21. Wang, W.L., Wang, T.T., Su, J.J., Lin, C.H., Seng, C.R., and Huang, T.H., (2001). "Assessment of damage in mountain tunnels due to the Taiwan Chi-Chi Earthquake." *Tunnelling and Underground Space Technology*, Volume 16, pp. 133-150.
22. Whitman, R. V., Reed, J. W., and Hong, S.-T. (1973). "Earthquake Damage Probability Matrices." *Proceedings of the 5th World Conference on Earthquake Engineering*, Rome, II, pp 2531–2540.